Aerosol layers from the 2008 eruptions of Mount Okmok and Mount Kasatochi: In situ upper troposphere and lower stratosphere measurements of sulfate and organics over Europe

J. Schmale, Jodi Schneider, T. Jurkat, C. Voigt, H. Kalesse, M. Rautenhaus, M. Lichtenstern, H. Schlager, Gérard Ancellet, F. Arnold, et al.

Aerosol layers from the 2008 eruptions of Mount Okmok and Mount Kasatochi: In situ upper troposphere and lower stratosphere measurements of sulfate and organics over Europe

J. Schmale,[1] J. Schneider,[1] T. Jurkat,[2] C. Voigt,[2,3] H. Kalesse,[3] M. Rautenhaus,[2] M. Lichtenstern,[2] H. Schlager,[2] G. Ancellet,[4] F. Arnold,[2,5] M. Gerding,[6] I. Mattis,[7] M. Wendisch,[8] and S. Borrmann[1,3]

Received 1 December 2009; revised 26 April 2010; accepted 28 April 2010; published 17 September 2010.

[1] In 2008 Mount Okmok and Mount Kasatochi started erupting on 12 July and 7 August, respectively, in the Aleutians, depositing emissions of trace gases and aerosols as high as 15.2 km into the atmosphere. During an aircraft campaign, conducted over Europe in between 27 October and 2 November 2008, the volcanic aerosol was measured by an Aerodyne aerosol mass spectrometer, capable of particle chemical composition measurements covering a size diameter range between 40 nm and 1 μm. In the volcanic aerosol layer enhanced submicron particulate sulfate concentrations of up to 2.0 μg m^{-3} standard temperature and pressure (STP) were observed between 8 and 12 km altitude, while background values did not exceed 0.5 μg m^{-3} (STP). Twenty-one percent of the volcanic aerosol consisted of carbonaceous material that increased by a factor of 1.9 in mass compared to the free troposphere. Enhanced gaseous sulfur dioxide concentrations measured by an ion trap chemical ionization mass spectrometer of up to 1.3 μg m^{-3} were encountered. An onboard radiation measurement system simultaneously detected an enhanced aerosol signal. Furthermore, two German lidar stations identified an aerosol layer before and after the campaign. Data analysis shows that the aerosol layer was observed mainly in the lowermost stratosphere. Correlation of particulate sulfate concentration and sulfur dioxide mixing ratios indicates that after a 3 month residence time in the stratosphere, not all sulfur dioxide has been converted into sulfate aerosol. The significant fraction of organic material might have implications on heterogeneous chemistry in the stratosphere, which need to be explored more thoroughly.

Citation: Schmale, J., et al. (2010), Aerosol layers from the 2008 eruptions of Mount Okmok and Mount Kasatochi: In situ upper troposphere and lower stratosphere measurements of sulfate and organics over Europe, *J. Geophys. Res.*, *115*, D00L07, doi:10.1029/2009JD013628.

1. Introduction

[2] Volcanoes are a sporadic but important source of stratospheric aerosol and precursor gases. Large eruptions like El Chichón (1982) or Mount Pinatubo (1991) emitted approximately 8 and 20 Mt of sulfur dioxide, respectively, into the stratosphere [*Krueger et al.*, 2008; *von Glasow et al.*, 2009] that was eventually converted into sulfate (or sulfuric acid) aerosol, temporarily enhancing the Junge aerosol layer. Especially after the Mount Pinatubo eruption, in situ aerosol measurements are available that quantify the additional particle surface area due to the volcanic aerosol [e.g., *Borrmann et al.*, 1993; *Jonsson et al.*, 1995; *Wilson et al.*, 1993]. In addition to the effects of the volcanic aerosols on radiation and climate the particles offer surface and volume for heterogeneous reactions [*Arnold et al.*, 1990; *Borrmann et al.*, 1997; *Fahey et al.*, 1993] and act as nuclei for the formation of polar stratospheric clouds [*Thomason and Peter*, 2006]. In particular, for the layers directly in the vicinity of the mid latitude tropopause heterogeneous effects of cirrus and volcanic aerosol enhancements may influence the ozone abundance and thus the radiative budget [*Borrmann et al.*, 1996; *Solomon et al.*, 1997; *Voigt et al.*, 2006]. For the descending aerosol layer after the 1991 Mount Pinatubo eruption *Keim et al.* [1996] showed based on midlatitude in situ measurements that NO_x can be reduced to almost

[1]Particle Chemistry Department, Max Planck Institute for Chemistry, Mainz, Germany.
[2]Deutsches Zentrum für Luft- und Raumfahrt, Institut für Physik der Atmosphäre, Oberpfaffenhofen, Germany.
[3]Institute for Atmospheric Physics, J. Gutenberg University, Mainz, Germany.
[4]LATMOS, Université Pierre et Marie Curie, Paris, France.
[5]Max Planck Institute for Nuclear Physics, Heidelberg, Germany.
[6]Leibniz Institute for Atmospheric Physics, Kühlungsborn, Germany.
[7]Leibniz Institute for Tropospheric Research, Leipzig, Germany.
[8]Institute of Meteorology, University of Leipzig, Leipzig, Germany.

0148-0227/10/2009JD013628

zero near the thermal tropopause on account of heterogeneous processing. The influence of such chemistry on ozone is still under debate [*Smith et al.*, 2001] and quantification of its magnitude and frequency of occurrence still remains open. The efficiency of heterogeneous reactions largely depends on the chemical composition and size of the aerosol particles involved. Reaction rates (e.g., for N_2O_5) depend most significantly on aerosol particles when the surface area is between 2 and 5 μm^2 cm^{-3} [*Fahey et al.*, 1993]. Thus, a small enhancement of reactive particles as provided by volcanic eruptions can increase the reaction rates efficiently in the upper troposphere and lower stratosphere (UT/LS) [*Griffiths et al.*, 2009; *Sander et al.*, 2006]. For these reasons direct in situ measurements of the particulate chemical composition are of high value. This is in particular the case for the tropical UT/LS where post eruption volcanic aerosols have been shown to contain significant amounts of non volatile material [*Borrmann et al.*, 2010] and where low temperatures enhance heterogeneous processing [*Popp et al.*, 2007; *Voigt et al.*, 2007]. Comprehensive summaries of the issues in connection with volcanic aerosols are provided by SPARC und WMO ozone assessments [*Thomason and Peter*, 2006; *World Meteorological Organization*, 1999] including extensive referencing and by *von Glasow et al.* [2009].

[3] New methods, such as aerosol mass spectrometry, have been developed in recent years and are now used to measure particle composition in the UT/LS, beginning with the works of *Murphy et al.* [1998] who was the first to operate a single particle mass spectrometer in the stratosphere. This type of laser ablation single particle mass spectrometer has since then been employed repeatedly, recently also in the tropical UT/LS region [*Froyd et al.*, 2009a, 2009b]. The bulk composition of polar aerosol has been detected in the lower stratosphere by balloon borne aerosol mass spectrometry [*Arnold et al.*, 1998; *Schreiner et al.*, 2002; *Voigt et al.*, 2000] in the UT/LS. A similar mass spectrometric technique, the Aerodyne aerosol mass spectrometer (AMS), that is able to quantify the non-refractory submicron aerosol components was first operated on aircraft in the lower troposphere by *Bahreini et al.* [2003], followed by midlatitude UT/LS measurements by *Schneider et al.* [2006a] and later on several more occasions [*Crosier et al.*, 2007; *DeCarlo et al.*, 2008; *Dunlea et al.*, 2009; *Morgan et al.*, 2009].

[4] After the eruption of Mount Pinatubo, a relatively long period with low stratospheric aerosol load was observed that is considered to represent the volcanically quiescent background [*Borrmann et al.*, 2010; *Deshler*, 2008]. Although tropospheric mass spectrometric measurements of continuous volcanic sulfate emissions originating from Mount Popocatépetl and Mount Colima near Mexico City and Iceland, respectively, have been reported by *DeCarlo et al.* [2008] and *Ovadnevaite et al.* [2009], there has not yet been the opportunity to obtain direct in situ measurements of stratospheric volcanic aerosol by aerosol mass spectrometry. In the year 2000, airborne in situ measurements of aerosol number, size, and volatility were performed shortly after the Mount Hekla eruption [*Hunton et al.*, 2005; *Rose et al.*, 2006]. However, these measurements did not include in situ particle chemistry.

[5] In summer 2008, two volcanoes on the Aleutians erupted: The volcano Mount Okmok (53.40°N, 168.17°W) became active on 12 July, and Mount Kasatochi (52.18°N, 175.51°W) on 7 August. Both outbreaks were strong enough to inject trace gases and aerosol particles into the stratosphere [*Carn et al.*, 2008], up to about 15 km. The enhanced trace gas and aerosol load in the lower stratosphere due to these volcanic emissions has been observed by in situ and remote sensing measurements [e.g., *Martinsson et al.*, 2009; *Theys et al.*, 2009].

[6] In this paper we present aircraft based in situ measurements from the CONCERT campaign (CONtrail and Cirrus ExpeRimenT [*Voigt et al.*, 2010]) conducted between 27 October and 2 November 2008 of the particle chemical composition of an aerosol layer encountered directly above the local tropopause and compare the results to data from the unperturbed upper troposphere and the lower stratosphere. Lidar profiles show that this aerosol layer was observed over central Europe continuously, starting 34 days after the Kasatochi eruption. In an accompanying paper, *Jurkat et al.* [2010] discuss the modification of the trace gas distribution in the lowest stratosphere by the Kasatochi eruption based on aircraft measurements of SO_2, HCl and HNO_3 during the CONCERT campaign.

2. Measurements

[7] The data on submicron aerosol chemical composition and size distribution, CO, O_3, SO_2 and spectral upwelling radiances have been recorded by various instruments during two aircraft campaigns, POLARCAT-France and CONCERT-Chemistry. Aerosol composition measurements were performed using the Aerodyne aerosol mass spectrometer. The main results were obtained on board the DLR-Falcon within the CONCERT campaign between 27 October and 2 November 2008 during six flights. The operation base of the CONCERT campaign was Oberpfaffenhofen (48.07°N, 11.27°E), Germany. Flights were conducted mostly at altitudes between 8000 and 12000 m over central and western Europe between longitudes of 15°E and 14°W and latitudes of 48° and 55°N. On 28 and 31 October 2008, a tropopause fold over the North Atlantic near the Netherlands and between France and Ireland, respectively, was probed. During these measurement flights, an aerosol layer with enhanced particulate sulfate mass concentration was observed in the UT/LS region. To compare the recorded data with results prior to the volcanic eruptions of Mount Okmok and Mount Kasatochi on 12 July and 7 August, accordingly, data from the POLARCAT-France project was used. This campaign took place in June–July 2008 in Greenland as part of the International Polar Year activities. Flights were carried out with the French research aircraft ATR-42 in all directions around the base in Kangerlussuaq from 60° to 71°N and 40° to 60°W with a maximum altitude ceiling of 7600 m.

2.1. Aerosol Mass Spectrometer

[8] On both aircraft the same Aerodyne compact time-of-flight aerosol mass spectrometer (in short C-ToF-AMS, hereafter AMS) was used to measure the chemical composition and mass concentrations (in terms of sulfate (abbre-

viated as SO_4), nitrate (NO_3), ammonium (NH_4), organics (Org), and chloride (Chl)) of submicron aerosol particles [*Canagaratna et al.*, 2007; *Drewnick et al.*, 2005]. Briefly, aerosol is sampled through a critical orifice followed by an aerodynamic lens system, where the particles are focused into a narrow beam, concentrated and accelerated when entering the instrument's vacuum chamber. After passing a time-of-flight region in the vacuum chamber the particles impact upon an inverted cone of tungsten operated at about 600°C. On this vaporizer the particles are flash vaporized and the generated gas molecules are ionized by electron impact (70 eV) before the ions are extracted into a time-of-flight mass spectrometer. Via the difference of mass spectra recorded with a completely open and blocked aerosol beam, the mass concentration of nonrefractory particle chemical components can be determined. Chemical composition can also be provided size-resolved. For this purpose, a chopper, located at the exit of the aerodynamic lens, cuts the particle beam to determine the particle time of flight for the calculation of the aerosol vacuum aerodynamic diameter (d_{va}) [*DeCarlo et al.*, 2004]. Based on a "fragmentation table" [*Allan et al.*, 2004b] the mass spectra can be converted into mass concentration of chemical species (sulfate, ammonium, nitrate, organics, and chloride) at standard temperature and pressure (273 K, 1013.25 hPa). The standard AMS quantification procedure is described by *Allan et al.* [2003]. During both campaigns, the AMS was operated in the so-called general alternation mode when the recording of mass spectra (MS mode) and particle time of flight (PToF mode) happens sequentially. For POLARCAT, one data point corresponds to 30 s sampling time spending three times five seconds in each mode. For CONCERT, the time resolution is ten seconds with each mode recording half of the time. Additionally, a fast mass spectrum (FMS) mode with one second time resolution was applied during certain intervals. Details of the FMS mode are described by *Kimmel et al.* [2008]. Data reported here are 30 s averages for CONCERT and 120 s averages for POLARCAT. In order to assure quantitative measurements, the instrument's ionization efficiency was determined six and three times for POLARCAT and CONCERT, respectively.

[9] On each aircraft, the AMS was connected to a forward facing inlet for isokinetic sampling. For the DLR-Falcon, the inlet has been described by *Fiebig* [2001] and *Schneider et al.* [2006a]. The inlet extends 30 cm beyond the fuselage sampling the air outside the boundary layer of the aircraft. The upper cutoff diameter is larger than 1.3 μm and thus does not interfere with the upper cutoff diameter of the AMS inlet. Inside the aircraft, a 1.9 mm ID stainless steel tube of less than one meter length connected the aircraft inlet with the AMS pressure controlled inlet (PCI) system. To guarantee isokinetic sampling the flow rate through this tube was kept constant at 2.5 l/min. Since the PCI had a flow rate of only 1.2 l/min a bypass with a throughput of 1.3 l/min was installed not interfering with the sample flow. During POLARCAT, the AMS sampled from the French community aerosol inlet (CAI) fabricated by COMAT as described by *Brenguier et al.* [2008]. CAI is an isokinetic and isoaxial inlet with an estimated 50% transmission efficiency at 2.5 μm; thus, the AMS measurements are not impaired. The mass spectrometer was connected via a 4.4 mm ID stainless steel tube of approximately 2 m total length to the aircraft inlet.

2.1.1. Pressure Controlled Inlet System Characterization

[10] The employed PCIs have been built according to the design described by *Bahreini et al.* [2008]. The purpose of a PCI is to facilitate stable conditions in front of the AMS inlet lens to assure the operation of the aerodynamic lens under constant pressure. Instable pressure conditions would lead to changes in the lens transmission function and to different acceleration velocities in the aerodynamic lens and thus to variability in particle sizing. Four modifications of PCIs were used during CONCERT and POLARCAT. A detailed description of the setup and functioning is provided in Appendix A. For correct quantification of particle mass, the transmission efficiency of the PCI was determined (for details see Appendix A) as shown in Figure 1. For PCI 1 to 3, deployed during CONCERT, the transmission efficiency is the same as for the standard inlet within the calculated error range. Generally, transmission between 200 and 400 nm d_{va} particles for PCI POLARCAT and between 200 and 600 nm for all other inlets is close to 100%. Thus, the respective data of the CONCERT campaign have not been corrected for differences in inlet transmission. The POLARCAT inlet shows lower transmission for particle sizes smaller than 200 nm d_{va} and larger than 400 nm resulting in an overall inlet transmission of approximately 54% compared to the standard inlet. All acquired mass concentrations from POLARCAT have been corrected accordingly.

2.1.2. AMS Data Correction, Errors, and Limit of Detection

[11] Next to losses occurring in the inlet and lens system (E_L) and losses due to nonfocusing of nonspherical particles after having passed through the aerodynamic lens (E_S), there are certain types of particles which hit the heater and bounce off immediately (E_B). These particles are not vaporized and their mass is thus not accounted for. In order to compensate for these artifacts, the so-called collection efficiency (*CE*) factor, the product of all three effects ($CE = E_L * E_S * E_B$), was introduced [*Huffman et al.*, 2005]. It has been shown that a *CE* factor of 0.5 represents quite well the sampling of ambient aerosol as determined and applied in various field campaigns [e.g., *Allan et al.*, 2004a; *Drewnick et al.*, 2004; *Hings et al.*, 2007]. Based on this experience and the lack of opportunity to compare AMS mass concentrations to data recorded by other instruments, the *CE* factor was assumed to be 0.5 for data reported here. An additional argument in favor of this value is that particles were sampled at ambient temperatures between −30 and −64°C at low relative humidity most of the time. Since the sampling line in the aircraft was not cooled, temperature differences between the outside and inside were on average 79 K with a maximum difference of 107 K. Thus, it is assumed that most of the water contained in the particles had been evaporated within the sampling line. So particles entering the AMS were dry and would therefore bounce of the heater more likely. Studies by *Matthew et al.* [2008] have shown that more solid phase particles have low collection efficiencies around 20%–30% opposed to liquid phase particles with *CE*s around 100%. On the other hand, it was found that very acidic aerosol mainly composed of sulfuric acid tends to

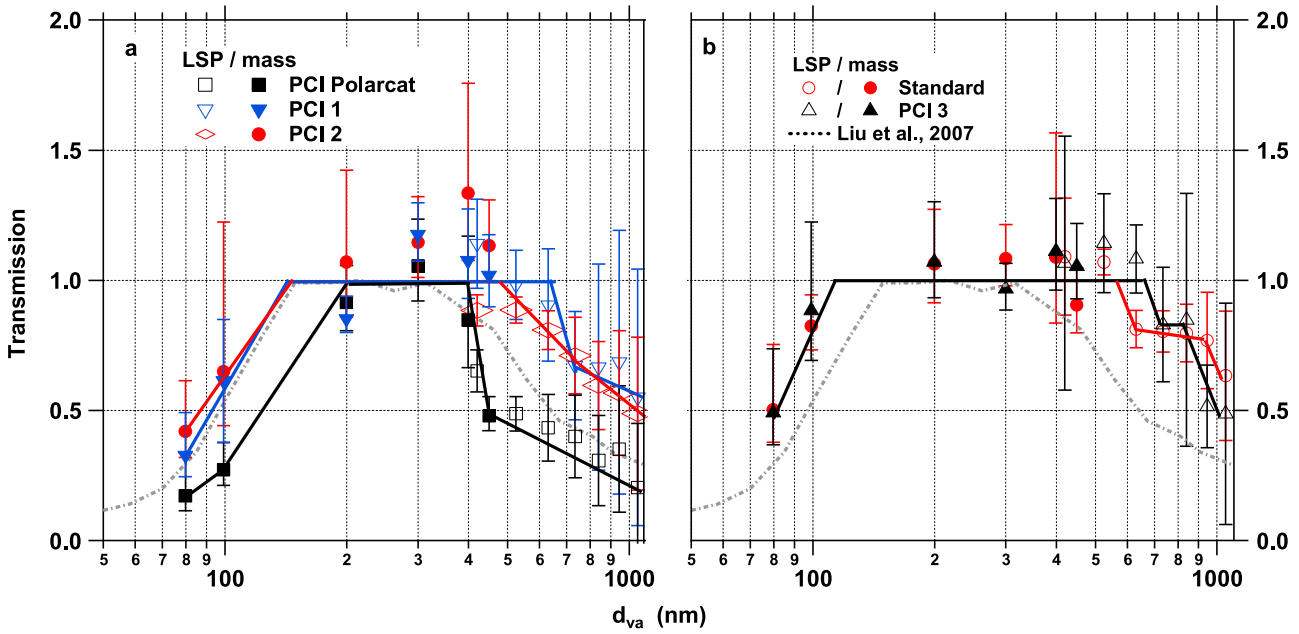

Figure 1. Measured particle transmission efficiency of AMS inlets. (a) Pressure controlled inlets (PCI) 1 and 2 used in CONCERT compared to the PCI used in POLARCAT. (b) Comparison between PCI 3 used in CONCERT, AMS standard inlet, and data from *Liu et al.* [2007]. For details on the PCIs, see Table A1. The error bars represent the standard deviation of 1 min averaged CPC counts over LSP counts for the total number of collected data points (15–20) with the LSP counting method. For the mass method, error bars denote variations in the charge probability of the monodisperse aerosol and counting statistics from AMS nitrate determination. Transmission efficiencies are around 100% from 200 to 400 nm for PCI POLARCAT and from 200 to 600 nm for all other PCIs and the standard inlet. Lines between the points were drawn only to guide the eye.

have a CE of 1 in a marine environment [*Quinn et al.*, 2006]. Here we applied a *CE* of 0.5 for all CONCERT measurements, while for POLARCAT we used a CE_{PCI} of 0.5*0.54 = 0.27, including PCI transmission efficiency.

[12] Several corrections had to be applied to the data for proper quantification. The employment of a PCI implies that the recorded data refer to conditions at P_{PCI}. Conversion to STP conditions was done by the following equation:

$$C_{STP} = C_{AMS} \times Q_{meas}/Q_{CO} \times P_{STP}/P_{PCI}, \quad (1)$$

with C_{STP} being the concentration at STP conditions, C_{AMS} the mass concentration obtained after standard AMS data processing, Q_{meas} the measured flow rate by the instrument, Q_{CO} the nominal flow rate through the last critical orifice, and P_{STP} being equal to 1013.25 hPa. Furthermore, the relative ionization efficiencies (*RIE*) of sulfate, ammonium, and organics relative to nitrate were found to be different from standard assumptions. Therefore, these values were determined in laboratory experiments for each flight's electronic acquisition settings. 350 nm particles were generated from a solution of known ratio of ammonium nitrate, ammonium sulfate and succinic acid, dried by two diffusion dryers and measured by the AMS in mass spectrum mode. By dividing the original mass composition ratio by the ratio obtained from the AMS the correct RIE values were determined. The average values are: RIE_{SO4} = 0.98 ± 0.03, RIE_{NH4} = 3.11 ± 0.05, and RIE_{Org} = 1.76 ± 0.02. Third, different electronic acquisition settings for general alternation and fast mass spectrum mode had to be compensated. Thus, the same laboratory generated particle types were measured by the AMS in both modes with each flight's instrumental settings. Division of the FMS mode values by the general alternation mode values yields the correction factor for each species.

[13] For each AMS data point an error has been calculated. It comprises uncertainties derived from counting statistics [*Allan et al.*, 2003] and for sulfate containing particles additionally an uncertainty of 5.2% due to variations in the relative ionization efficiency caused by temperature fluctuations of the heater. Other species were found not to be affected by this effect. The systematic error due to the collection efficiency cannot be determined on a point by point basis. The uncertainty in the transmission efficiency related to the PCI is in the order of 30% (see Figure 1) but not significantly higher than for the standard inlet. In Figure 3, exemplary error bars are shown accounting for this general uncertainty.

[14] The limit of detection (LOD) has been calculated as three times the standard deviation of the closed signal of each aerosol species, multiplied by √2 [*Drewnick et al.*, 2009]. For aircraft measurements special circumstances apply, meaning that the instrument's vacuum can only be established within a short time period before takeoff, i.e., approximately 4 h for POLARCAT and CONCERT campaigns. Therefore, background concentrations of certain m/z are elevated compared to levels after long pumping periods. Thus, the pumping during the flight still has a significant

Table 1. Limit of Detection (μg m^{-3}, STP) per Flight During CONCERT for 30 s Average Data

Flight	SO_4	NO_3	NH_4	Org	Chl
27 Oct 2008	0.02	0.03	0.12	0.14	0.04
28 Oct 2008	0.03	0.02	0.17	0.11	0.04
29 Oct 2008	0.02	0.03	0.10	0.10	0.03
31 Oct 2008a	0.03	0.02	0.13	0.10	0.03
31 Oct 2008b	0.02	0.02	0.13	0.07	0.03
2 Nov 2008	0.02	0.02	0.15	0.11	0.03

impact on these background loadings and concentrations are reduced in the course of the flight. On average the pumping time during the flight is as long as the preparation period before the flight. This results in a long-term trend in the background signal on which noise is superimposed. Using the standard deviation from the closed signal background would thus yield an overestimated detection limit. To compensate for this effect, an algorithm has been applied that allows for calculation of the standard deviation of a signal that is a combination of short-scale noise and a long-scale trend. This algorithm is described in detail by P. Reitz and J. Schneider (Noise level determination by local cubic signal approximation: Calculation of Aerodyne aerosol mass spectrometer detection limits, submitted to *Atmospheric Measurement Techniques Discussion*, 2010). It uses a local cubic approximation of the long-scale variation of the signal in order to separate them from the short-scale variations which contain the information on the noise of the curve. The output of the algorithm corresponds to the standard deviation of the noise of the signal. LODs during CONCERT have been determined for 30 min intervals of each flight. Average limits of detection of 30 s average data are given in Table 1. These values show that the level of significance is in the order of 0.01 μg m^{-3}.

2.2. Further Instruments Aboard DLR-Falcon

[15] Ozone measurements were performed with a two cell (zero, sample) UV absorption photometer switching chambers every four seconds. Pressure and temperature data were also recorded by the instrument at a 1 Hz rate. Ozone values are generated every four seconds. This data is then corrected for pressure and temperature. The range of the instrument is 0 to 1000 nmol mol^{-1} with a detection limit of 1 nmol mol^{-1} [*Brough et al.*, 2003]. Carbon monoxide measurements are based on fluorescence detection. The instrument can be operated to less than 100 mbar and has been calibrated regularly during flights by injection of a known CO standard. The time resolution is one second and response is linear between 0 and 1000 mmol mol^{-1} while the detection limit is smaller than 6 nmol mol^{-1} and precision is 1.5 nmol mol^{-1} [*Brough et al.*, 2003].

[16] Sulfur dioxide measurements were performed with an IT-CIMS (ion trap chemical ionization mass spectrometer) [*Fiedler et al.*, 2005; *Speidel et al.*, 2007; *Fiedler et al.*, 2009]. The IT-CIMS instrument was equipped for the first time with an SF_5^- ion source using a selective reaction for the detection of SO_2. HNO_3 and HCl can be detected simultaneously by the instrument [*Marcy et al.*, 2005]. The time resolution of the instrument is 1.6 s. Calibration was performed during the flight for HNO_3 and after the flights for SO_2 and HCl. The detection limit for a running mean over 10 spectra is 18 pptv for SO_2 and 22 and 36 pptv for HCl and HNO_3 (for a running mean over 20 spectra), respectively. A detailed description of the instrument is given in an accompanying paper by *Jurkat et al.* [2010].

[17] Spectral upwelling radiation data was obtained with the Spectral Modular Airborne Radiation measurement sysTem (SMART)-Albedometer [*Wendisch et al.*, 2001]. For the CONCERT experiment two optical inlets designed to measure radiances $I_\lambda^\uparrow$ and irradiances $F_\lambda^\uparrow$ were installed in the rear of the fuselage of the aircraft pointing downward to measure upwelling radiation. The inlets were each connected via optical fibers to a pair of grating spectrometers operating in the wavelength ranges 350–1050 nm and 900–2200 nm with spectral resolutions (full width at half maximum, FWHM) of 2–3 nm and 9–16 nm, respectively. The design of the radiance inlet with an opening angle of 2.1° is described by *Ehrlich et al.* [2008]. The performance of the SMART-Albedometer on the Falcon aircraft in high-altitude conditions has been demonstrated in a previous flight experiment [*Eichler et al.*, 2009]. The temporal resolution of the radiance measurement was set to 1 s leading to a spatial averaging of 200 m at an aircraft velocity of 200 m s^{-1}. Resulting total relative errors are wavelength dependent and are in the range of 6%–9%.

2.3. Further Instruments Aboard ATR-42

[18] The ATR ozone detection instrument is based on UV absorption with two cells. It has a precision of 2 nmol mol^{-1} and a time resolution of four seconds. More detailed information can be obtained from *Ancellet et al.* [2009].

2.4. Additional Data Sets

[19] For supplementary analysis, potential vorticity (PV) was calculated from ECMWF (European Centre for Medium-Range Weather Forecasts) analysis data to obtain information about the height of the tropopause as estimated from the 2-PVU (potential vorticity units) isosurface [*Holton et al.*, 1995]. ECMWF analyses were available four times daily (00, 06, 12 and 18 UTC) at a resolution of 0.25 degrees in the horizontal and 91 hybrid sigma-pressure levels in the vertical direction. For comparison with the measurements, we interpolated the model PV linearly in time and space to the Falcon flight track.

[20] Additional AMS particulate sulfate and ozone mixing ratio data have been used from the 60 s merged data set archive of the ARCTAS campaigns in spring and summer 2008. These two experiments were part of the International Polar Year project and took place in Alaska and Canada, chronologically. Since the objectives were detection of Arctic haze in spring and influence of biomass burning in summer, data representing pollution conditions had to be filtered. This was achieved by applying a 0.2 nmol mol^{-1} acetonitrile [*Warneke et al.*, 2006] and a 80 nmol mol^{-1} carbon monoxide upper threshold to exclude anthropogenic and biomass burning influences. To obtain data from only above the troposphere an empirical definition for the tropopause lower boundary based on ozone mixing ratio was used [*Zahn and Brenninkmeijer*, 2003].

[21] Further Aerosol data were provided by the EARLINET lidar stations at Kühlungsborn (54°N, 12°E, Rayleigh-Mie-Raman) and Leipzig (51°N, 12°E, Raman). These data

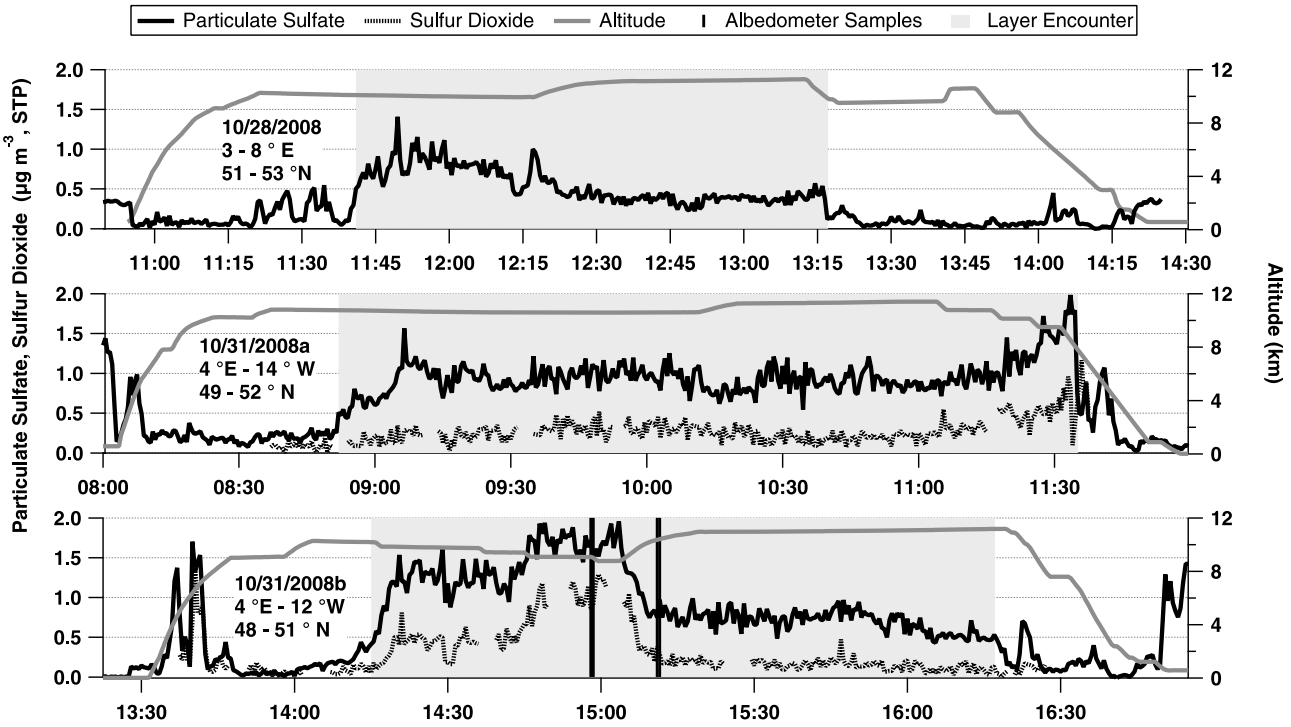

Figure 2. Time series of the elevated particulate sulfate loadings during three flights and increased sulfur dioxide concentrations during two flights in October 2008 when the volcanic aerosol layer was encountered (shaded areas). The vertical lines in Figure 2 (bottom) indicate the discussed sampling periods by the SMART-Albedometer.

represent aerosol backscatter coefficients (sr^{-1} Mm^{-1}) at 532 and 1064 nm, respectively.

3. Results and Discussion

3.1. Identification of a Volcanic Aerosol Layer

[22] During one flight on 28 October and two flights on 31 October 2008, unusually high concentrations of particulate sulfate were measured over the North Sea (3–8°E, 51–53°N) and the North Atlantic (4°E–14°W, 49–52°N, and 4°E–12°W, 48–51°N), respectively. Figure 2 shows the time series including particulate sulfate concentrations, sulfur dioxide mixing ratios, and altitude. Encounters of the aerosol layers, marked by shaded areas, are characterized by a rapid increase in sulfate aerosol concentration while it decreases steeply when leaving the layer. More than 50% of each displayed flight has been spent within the aerosol layer. During several periods at altitudes above 8 km, particulate sulfate was enhanced, with mean values and standard deviations of 0.54 ± 0.22, 0.82 ± 0.36 and 0.79 ± 0.50 $\mu g\ m^{-3}$ (STP), in chronological order with a maximum observed value of 1.98 $\mu g\ m^{-3}$. The mean value in the boundary layer for all flights was 0.50 $\mu g\ m^{-3}$ (STP) and thus lower than the mean values above 8 km which is a strong indication for an exceptional layer encounter in the UT/LS. The fluctuations in particulate sulfate mass loadings as shown in Figure 2 can be ascribed to inhomogeneity of the aerosol layer if they are greater than 8% of the actual measurement value. This estimation is based on the counting statistics error of each data point. Thus, the time series show that the encountered aerosol layer was not completely homogeneous. During the measurement flights on 27 and 29 October and 2 November 2008, mean sulfate loadings at the same altitudes were always below 0.17 $\mu g\ m^{-3}$. The high values on 28 and 31 October are remarkable especially when considering earlier AMS airborne measurements over Germany in 2003 [*Schneider et al.*, 2006a] and over the UK region in 2005 and 2006 [*Morgan et al.*, 2009], both showing significantly lower concentrations. According to the latter measurements, the average particulate sulfate concentration above 8 km was about 0.39 $\mu g\ m^{-3}$ for all recorded vertical profiles, while for the free troposphere between 3 and 8 km the average was 0.23 $\mu g\ m^{-3}$. This value is consistent to our findings in the free troposphere with 0.22 $\mu g\ m^{-3}$ for all CONCERT flights.

[23] Figure 2 also shows that particulate sulfate and gaseous sulfur dioxide concentrations are well correlated throughout the two flights on 31 October. Elevated particulate sulfate concentrations are accompanied by elevated SO_2 concentrations. The enhanced SO_2 values in the aerosol layer show that during the residence time of the air mass in the atmosphere SO_2 has been converted to certain extent into sulfate aerosol but not entirely.

[24] High particulate sulfate loadings between 8 and 12 km can result from various types of emissions. The observed sulfur dioxide might have been emitted by local air traffic, and sulfate aerosol can be produced by conversion of sulfur dioxide into sulfuric acid containing particles. Also,

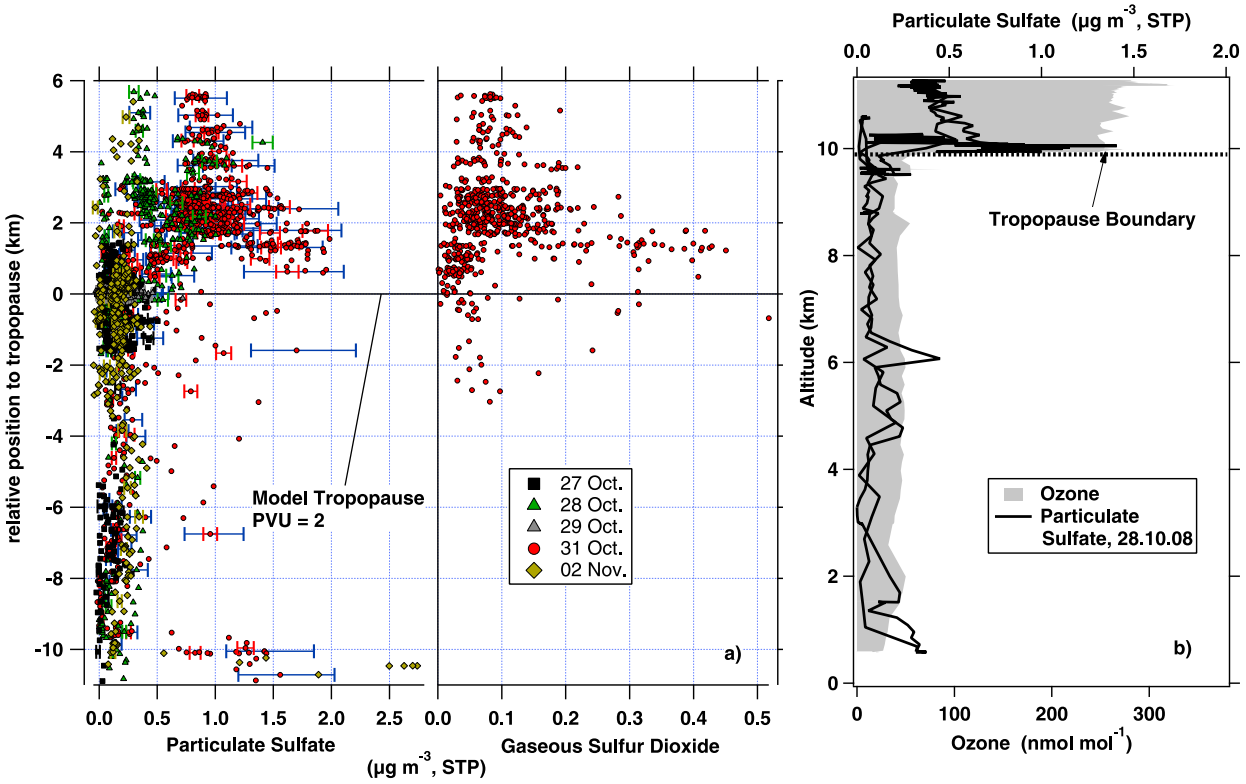

Figure 3. (a) Entire campaign vertical profile of particulate sulfate and gaseous sulfur dioxide (only 31 October) relative to the ECMWF model tropopause boundary at 2 PVU. The exemplary blue error bars plotted along with the sulfate data represent the general AMS measurement uncertainty of 30%; the error bars in symbol color represent the statistical uncertainty. (b) Vertical profile of particulate sulfate and ozone on 28 October.

convective vertical transport of surface emissions might be responsible for the elevated sulfur concentrations. A third explanation is injection of sulfur dioxide into the stratosphere by volcanic eruptions, with subsequent conversion of SO_2 to particulate sulfate, causing aerosol layers that can remain several months in the lower stratosphere above the tropopause [*Borrmann et al.*, 1993]. Regarding the first argument, CONCERT data indicates that air traffic emissions are not responsible for this aerosol layer, although it was encountered in the heavily trafficked North Atlantic flight corridor. Data from measurements directly in contrails of regular aircraft traffic do not show values higher than 0.51 μg m^{-3}, see Figure 3a (27 and 29 October, 2 November), and have a much lower average value, i.e., 0.17 μg m^{-3}.

[25] In order to test for recent or potentially high reaching contributions from the surface other than volcanoes, trajectories were computed with HYSPLIT [*Draxler and Rolph*, 2003]. However, the results indicate that the air masses in the area in question did not originate from low altitudes in the 10 days prior to the encounter. The model was run with the GDAS global data set. For the three flights of 28 and 31 October, trajectories were initialized at horizontal coordinates taken in 15 min intervals from the flight track. Initial altitudes were set to 8, 10, and 12 km, as the actual flight altitude within the aerosol layers varied between 10300 and 10700 m. Computations were started at the time of the observations and additionally 3 h earlier and 3 h later and were run backward in time. The evaluation of 234 trajectories shows that 79% of the tracked air parcels stayed at constant altitudes between 10 and 14 km. Only 21% of the trajectories encountered altitudes below 6 km before arriving at the aircraft location, but most of them were launched at the 8 km level, below the actual aircraft altitude. The 12% of the total number of computed trajectories that dropped below 4 km were almost exclusively launched at 8 km. Hence, the trajectory simulation strongly suggests that surface emissions are not responsible for the observed sulfate concentrations.

[26] Thus, the only remaining explanation for the observed aerosol layer is that sulfur was injected into the atmosphere by volcanic emission. However, since the volcanic eruptions of Mount Okmok and Mount Kasatochi had already occurred in July and August 2008, respectively, the only plausible explanation why the volcanic emissions and their conversion products survived until the end of October is that they had reached the stratosphere. Upper tropospheric sulfate aerosol would have been removed by cloud processes [*von Glasow et al.*, 2009]. In order to investigate whether the aerosol layer was located above or below the tropopause, we used the dynamic definition of the tropopause and set the threshold for its lower boundary to 2 potential vorticity units (PVU) [*Holton et al.*, 1995] from ECMWF model data. The

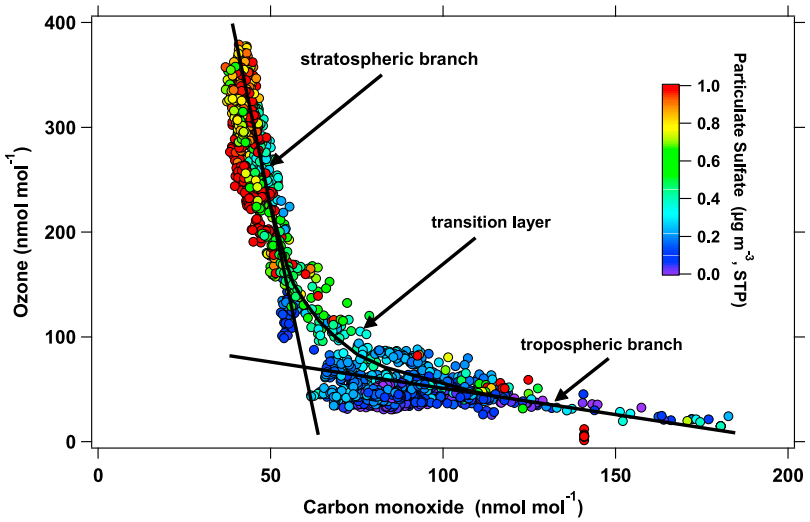

Figure 4. Scatterplot of O_3 versus CO, color coded by particulate sulfate concentration. Highest loadings occur in the stratospheric branch (high O_3) and partly also in the transition layer but not, however, in the tropospheric region (high CO).

tropopause altitude varied strongly during flights with layer encounters from 250 to 550 hPa, whereas it was located between 200 and 300 hPa for days without enhanced aerosol concentrations. Figure 3a shows particulate sulfate and gaseous sulfur dioxide displayed vertically as a function of altitude relative to the 2 PVU boundary, illustrating that the aerosol layer has been encountered solely above the tropopause. There is a clear difference in sulfate concentration between the three flights with layer encounters (28 and 31 October) and the three flights without encounters (27 and 29 October, 2 November). The mean concentration within the layer (PVU > 2) is 3.5 times higher (0.79 μg m^{-3}) than for background conditions. In the free troposphere (PVU < 2), values oscillate around similar means, i.e., 0.15 μg m^{-3} and 0.18 μg m^{-3} for background and layer, respectively. The sulfur dioxide data of 31 October also show enhanced concentrations above the 2 PVU boundary at the same altitude as particulate sulfur. *Jurkat et al.* [2010] calculated that for this day, 80% of the total sulfur had been converted into particulate matter.

[27] Figure 3b shows the sulfate aerosol and ozone mixing ratio vertical profile measured on 28 October as an example. The steep increase of the ozone mixing ratio from tropospheric values around 50 nmol mol^{-1} to stratospheric values of about 250 nmol mol^{-1} indicates the chemical tropopause. This plot additionally illustrates that the observed aerosol layer was located above the tropopause.

[28] Another approach to investigate where the layer was located with respect to the tropopause, is to consider tracer relationships [*Fischer et al.*, 2000] and [*Pan et al.*, 2004]. Even the aerosol measurements themselves can be used under certain circumstances as dynamical tracers as has been demonstrated by *Borrmann et al.* [1995] by studying the temporal evolution of the ozone versus aerosol correlation for the development of the Mount Pinatubo eruption plume. Here ozone (O_3) as a stratospheric tracer is plotted versus carbon monoxide (CO) as a tropospheric tracer in Figure 4. The lines indicate regions that belong to the stratosphere, troposphere and the transition region. Color coding the data points with particulate sulfate concentration provides an additional perspective on where exactly the layer has been encountered. The highest concentration of sulfate aerosol was observed in the stratospheric branch while lower concentrations were also encountered in the transition layer. However, no significant enhancement appeared in the tropospheric branch except for boundary layer data points.

[29] The finding that the layer is encountered only above the tropopause in the lower stratosphere is a strong indication that the sulfate aerosol layer is a result of a volcanic eruption that injected sulfur into the stratosphere. Mount Okmok (53.40°N, 168.17°W) and Mount Kasatochi (52.18°N, 175.51°W) in the Aleutians are known to have fulfilled this criterion. Mount Okmok started erupting on 12 July for approximately one month, Mount Kasatochi erupted on 7 and 8 August, 2008. Mount Okmok injected about 0.1 Tg SO_2 into the stratosphere up to 15 km, while Mount Kasatochi emitted 1.5 Tg SO_2 [*Carn et al.*, 2008] with a column height of 15.2 km (http://www.avo.alaska.edu/). The layer was thus probed between 108 and 111 days after the first eruption and 82–85 days after the second one. Comparison to measurements conducted by the CARIBIC platform before, during and after the eruption also supports the assumption that this layer was of volcanic origin [*Martinsson et al.*, 2009]. CARIBIC is a scientific project which deploys a freight container on commercial long-distance aircraft to study the atmosphere's chemical and physical processes. Figure 5 depicts a 2008 timeline of ratios of particulate sulfur concentrations and ozone mixing ratios. The most abundant data set is provided by filter sampling of sulfate and trace gas measurements of the CARIBIC platform. Particulate sulfur is analyzed in the laboratory by particle-induced X-ray emission (PIXE) of particle sizes between 0.07 and 1.5 μm [*Martinsson et al.*, 2001]. Even though particle sizes above 1 μm are taken into account, results are still comparable to AMS submicron measurements, since experience shows that more than 90% of the mass is carried by particles smaller than 0.6 μm [*Martinsson et al.*, 2005]. Ozone was measured by a UV absorption instrument. AMS particulate sulfate

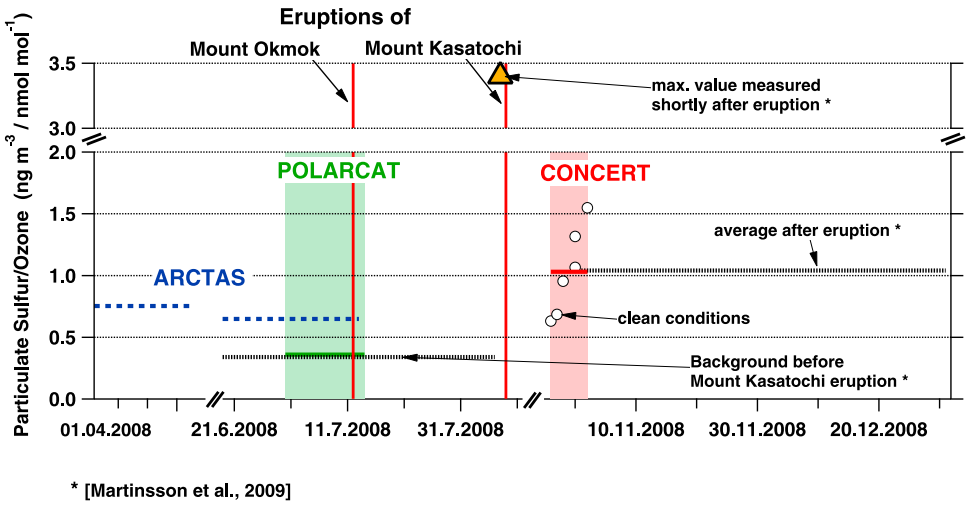

Figure 5. Chronological overview of particulate sulfur to ozone ratio in 2008 in the UT/LS including data sets from ARCTAS, POLARCAT, and CONCERT aircraft campaigns and CARIBIC data.

values were transformed into particulate sulfur loadings assuming that all sulfur was present as sulfate. According to the CARIBIC data, the average ratio of sulfur to ozone before the Kasatochi eruption for above troposphere data was 0.34 ng m^{-3} $nmol^{-1}$ mol (hereafter termed "units"), illustrated by the dashed line between 21 June and 6 August. Shortly after the eruption, the ratio peaked with 3.4 units (triangle) and then leveled out at 1.05 units beginning in October (dashed black line). CONCERT measurements in October show a mean value of 0.65 units for background conditions above the troposphere and 1.22 units within the volcanic layer. The average is indicated by the red solid bar while open circles refer to average values above 1.5 PVU per flight, which have an overall average of 1.03 units. Thus, general mean values determined during CONCERT are very close to findings by *Martinsson et al.* [2009] under the condition that the CE is assumed to be 0.5. To compare CARIBIC levels from before the eruption to other AMS measurements, data from POLARCAT and ARCTAS were consulted. The POLARCAT average value for the S/O_3 ratio is 0.36 units (solid green line July 2008), so very close again to CARIBIC findings. Tropopause and stratospheric background measurements obtained from ARCTAS show levels of 0.75 and 0.68 units for spring and summer, respectively, which is higher than the values from CARIBIC and POLARCAT before the eruption, but in good agreement to CONCERT background findings (outside the volcanic aerosol layer) and still significantly lower than the CARIBIC value after the eruption.

[30] Further indication for a volcanic origin of the layer provides a comparison to the particulate sulfur versus potential vorticity findings of *Martinsson et al.* [2005] based on CARIBIC data acquired at >8.2 km. They binned sulfur concentrations for volcanically quiescent periods in intervals of [0, 1], [1, 1.5], [1.5, 2.5], [2.5, 5], and [5, 7] PVU and found an average concentration of 15.9 ng m^{-3} for the first two intervals while concentrations increased linearly up to 62 ng m^{-3} at 7 PVU over the other three intervals. During CONCERT concentrations at 2 and 7 PVU were approximately 71 and 238 ng m^{-3}. A linear fit through the average value of each bin reveals that the slope after the Kasatochi eruption is roughly a factor 4 higher than during "clean" periods between 1999 and 2002 (Figure 6). The uncertainty of the AMS data due to the assumed collection efficiency of 0.5 is by far not large enough to explain the different slopes of the data sets.

[31] Figure 7 shows a cross section of the observed tropopause fold on 28 October at 12 UTC based on ECMWF analysis. The dashed red line indicates the 2 PVU boundary, the color coded thick solid line represents the particulate sulfate concentrations along the flight track. A distinct increase in the sulfate aerosol concentration is visible above the 2 PVU threshold. The elevated concentrations were first observed after the Falcon had reached the dynamic tropopause at around 11:15 UTC. For the flight leg between 13:12 and 13:40 UTC, slightly below the 2 PVU line, the concentration decreased to CONCERT-typical free tropospheric values of below 0.2 μg m^{-3} (STP).

[32] The aerosol layer was observed not only by the AMS during CONCERT campaign but also by the SMART-Albedometer on board the Falcon aircraft during the flight on 31 October from Shannon, Ireland to Oberpfaffenhofen, Germany. Over the Northeastern Atlantic approximately 100 km off the English coast, the aerosol layer was detected most clearly. Before and after the aerosol layer encounter, measurements were made in clear air conditions. Small scattered cumulus clouds discernable by pronounced peaks in the time series of $I_\lambda^\uparrow$ were present all along the flight track. Times during which the highly reflective low-level clouds were detected have been removed from the data time series. Spectra of $I_\lambda^\uparrow$ in the wavelength range 350–1000 nm are presented in Figure 8. Measurements in clear sky conditions made at 15:11 UTC during a 15 s time span during which no clouds were beneath the aircraft were averaged and are displayed in black. Measurements of $I_\lambda^\uparrow$ within the haze layer obtained at 14:58 UTC are shown in green (see Figure 2 (bottom) for indication of sample periods). Data were averaged over the 30 s time span during which no clouds contaminated the signal. Between the two measurements, the solar zenith angle (SZA) changed from 73.4° to 75.9°.

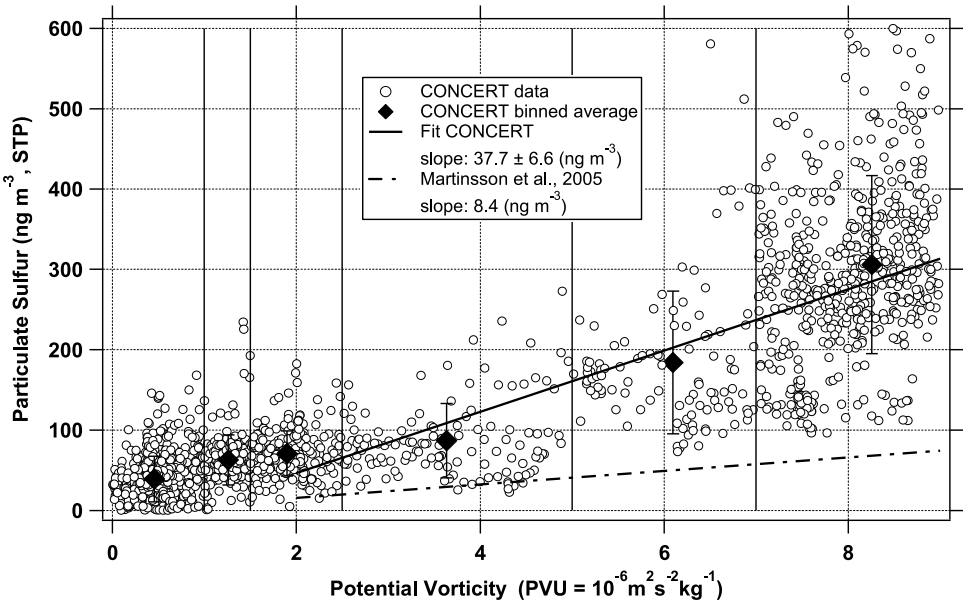

Figure 6. Comparison of particulate sulfur concentrations found by *Martinsson et al.* [2005] during volcanically quiescent periods from 1999 to 2002 with data from 82 to 85 days after the Kasatochi eruption. Open circles show all CONCERT data points above 8.2 km altitude; the diamonds are averages of the these data within PVU bins, which are represented by the vertical solid bars. The error bars denote the standard deviation within the bin.

To allow for a comparison of the measured spectra, $I_\lambda^\uparrow$ observed at 14:58 UTC were rescaled to SZA = 75.9°. Figure 8 shows that the mean $I_\lambda^\uparrow$ spectra measured in clear sky conditions are higher than the mean spectrum obtained when the aircraft was flying within the haze layer. However, differences are wavelength dependent. While at 500–600 nm the clear sky $I_\lambda^\uparrow$ is 28% higher than the signal measured in the haze layer, it is only 17% higher at 600–

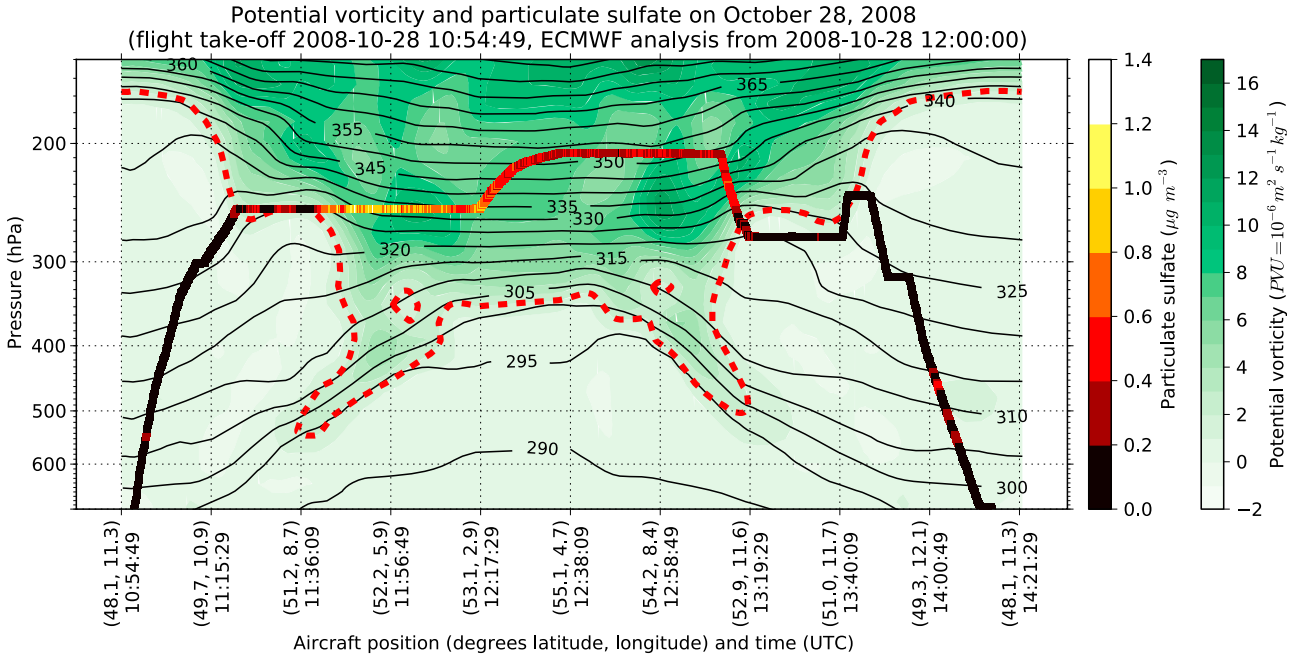

Figure 7. Vertical cross section of ECMWF analyzed potential vorticity on 28 October 2008, 12 UTC along the flight route. The height of the tropopause as estimated from the 2-PVU isosurface is highlighted by the dashed red line. The flight profile is color coded with the particulate sulfate concentration (μg m^{-3} STP). Note the elevated concentrations above the tropopause. The thin black lines show potential temperature (K).

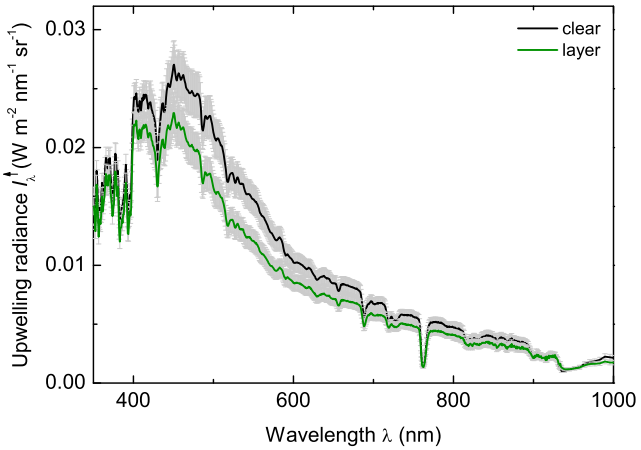

Figure 8. Mean spectral upwelling radiances $I_\lambda^\uparrow$ in clear-sky and volcanic haze layer conditions. The shaded areas correspond to the measurement and calibration uncertainties.

800 nm which can be attributed to the scattering properties of the aerosol layer. The aircraft flew approximately 1.7 km above the tropopause when this radiance spectrum was obtained. From Figure 3 we can conclude that the aerosol layer resided on average about 0.5 km above the dynamical tropopause. Thus, the vertical extension of the aerosol layer below the aircraft was roughly 1.2 km.

[33] A 5 K temperature increase within the haze layer was measured. However, based on the available data set it is not possible to attribute this warming solely to absorption by the aerosol. Information about the aerosol scattering properties (volume extinction coefficient or aerosol optical thickness, single-scattering albedo, and asymmetry parameter) would be required to simulate up-welling and downwelling irradiances above and below the aerosol layer which in turn would be needed to calculate local solar heating rates [*Wendisch et al.*, 2008].

[34] From AMS measurements it is known that 71% of the aerosol was composed of particulate sulfate, a weakly absorbing component, and 21% of carbonaceous material (see section 3.2). However, possible refractory absorbing components were not measured. Heating rates of approximately 7 K/d have been observed before by *Wendisch et al.* [2008]. However, that study was based on measurements of aerosol layers with a significant amount of soot with a particle single-scattering albedo of 0.85. Due to the lack of information on absorbing material we cannot determine whether local absorption of solar radiation contributes partly to the observed temperature increase which is mainly caused by thermodynamic effects due to the tropopause folding.

[35] Several EARLINET lidar stations observed the haze layer. In Figure 9 data from two German stations, Kühlungsborn and Leipzig, together with two AMS sulfate particle concentration vertical profiles are shown. Twenty-three days after the eruption, a layer around 18 km was observed. In the period from 34 to 78 days later, a layer was found at lower altitudes with a peak at 12 km by both lidar stations as highlighted by the shaded area. The data at day 78 show an average of about 30 min for altitudes between 11 and 13 km, while above data are averaged over all night for the Kühlungsborn lidar. The Leipzig lidar suggests also a second layer at higher altitudes around 17 km which was also observed on previous days at both stations. The CONCERT aircraft measurements on day 82 show that the layer had descended to 10 km and by day 85 to 8 km. Based

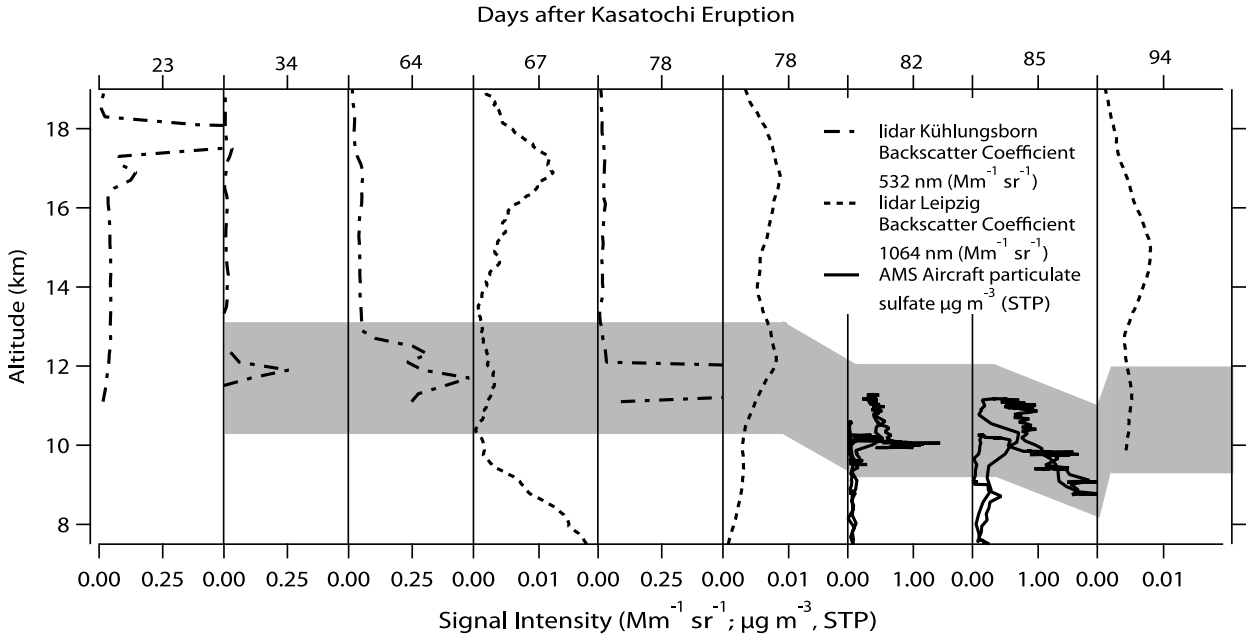

Figure 9. Time series of lidar and AMS aerosol vertical profiles after the Mount Kasatochi eruption. Signal intensity represents the backscatter coefficient (Mm^{-1} sr^{-1}) for lidar data and mass concentration (μg m^{-3}) for AMS data on linear axes. The shaded area highlights the observed volcanic aerosol layer in the UT/LS.

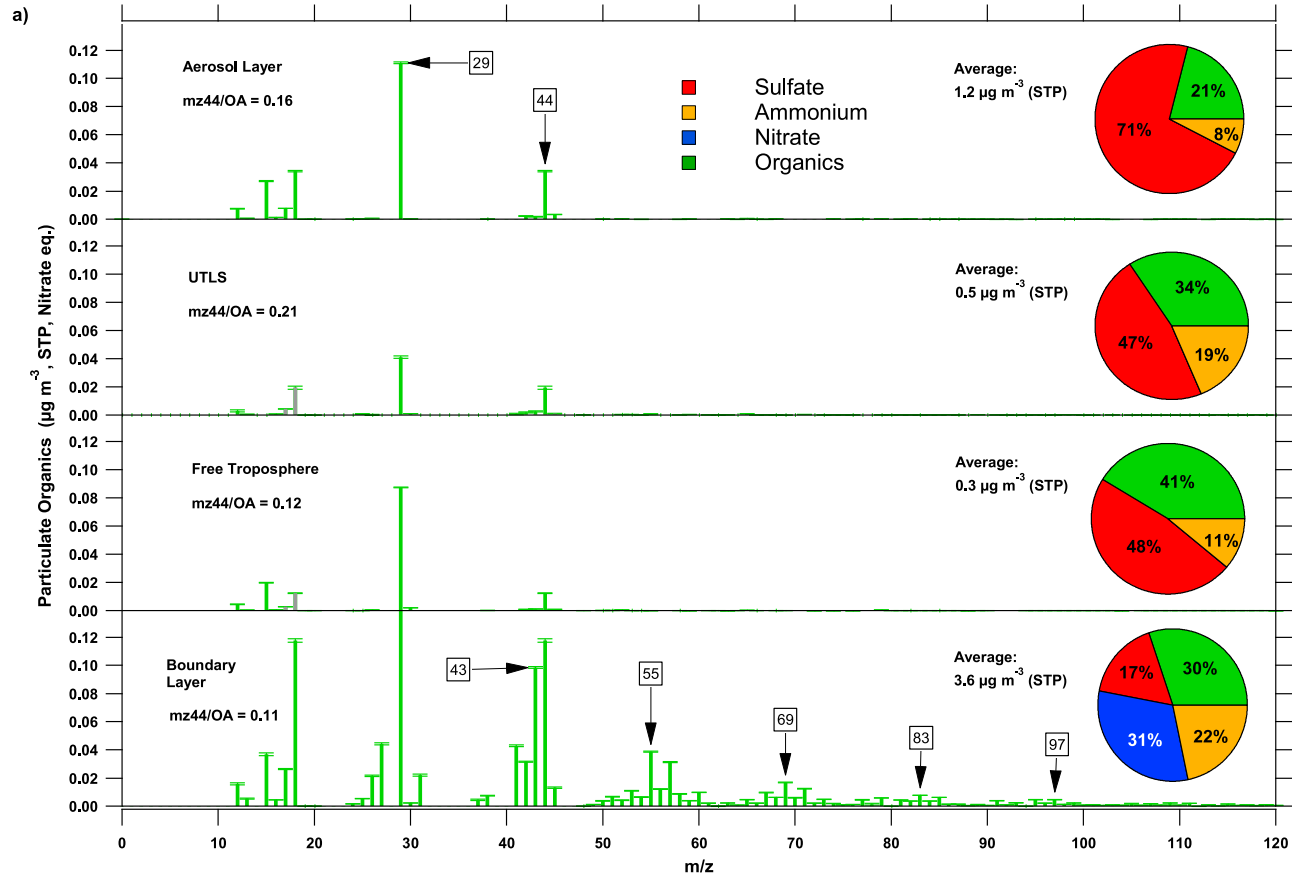

Figure 10. (a) Organic mass spectra at different atmospheric layers with degree of oxidation shown by the ratio of mass 44 over total organic mass (OA). Error bars on m/z sticks denote uncertainties from counting statistics, while gray bars represent values below detection limit. The pie charts indicate the relative contributions from organics, sulfate, ammonium, and nitrate to the submicron particulate phase. The average mass concentration for each layer is indicated. (b) The size distributions represent the total AMS aerosol in the boundary layer and the sulfate aerosol in the volcanic layer.

on particle sedimentation alone such vertical distances can be covered in the given time frame only by particles with size diameters above 3 μm according to settling velocity calculations after *Hinds* [1999]. Typically, particles this large are not encountered in the stratosphere as data from after the Mount Pinatubo eruption show where the largest sizes were around 1 μm. Meteorological data like potential vorticity as well as O_3 and CO measurements suggest that this subsidence was caused by a tropopause fold. The last profile shows the layer again at 12 km with a second one more pronounced around 15 km.

[36] The encountered aerosol layer had a vertical thickness of about 2 km (see Figure 3 and Figure 9). The horizontal extension can only be estimated roughly: The almost continuous observations of the layer by the two lidar stations suggest that the layer was distributed equally around the globe in the northern hemisphere. If we assume a south-north extension of about 45°N to 75°N, this corresponds to a volume of about 1.32×10^8 km^3. With the measured average particulate sulfate concentration of 0.8 μg m^{-3} (STP) and a molar fraction of 80% sulfate in total sulfur, we can estimate that the total sulfur content of the layer is 0.01 Tg S. The amount of sulfur deposited by Mount Kasatochi and Mount Okmok in the stratosphere was estimated to be 0.8 Mt (1.6 Mt SO_2); thus, this estimate suggests that about 1% of the total sulfur that was deposited by the two volcanoes in the stratosphere is confined in the observed aerosol layer in the lower stratosphere. Although this estimation is very rough and can easily be wrong by a factor of two or more, it shows that the layer contained only a small fraction of the total sulfur from the two volcanoes. The second aerosol layer observed by the lidar stations at about 16–18 km (Figure 9) may contain about the same amount of sulfur. This implies that either a large fraction has already been removed by stratosphere to troposphere air mass exchange, i.e., tropopause folding and quasi-horizontal transport, followed by wet deposition in the upper troposphere, or that a significant fraction of volcanic aerosol in the stratosphere cannot be detected and goes unnoticed by remote sensing and in situ observations.

3.2. Aerosol Characteristics

[37] Aerosol chemical composition and size distributions were recorded for every flight. Figure 10a shows the relative contribution of chemical species to aerosol in three distinct layers of the atmosphere. Encounters with the volcanic

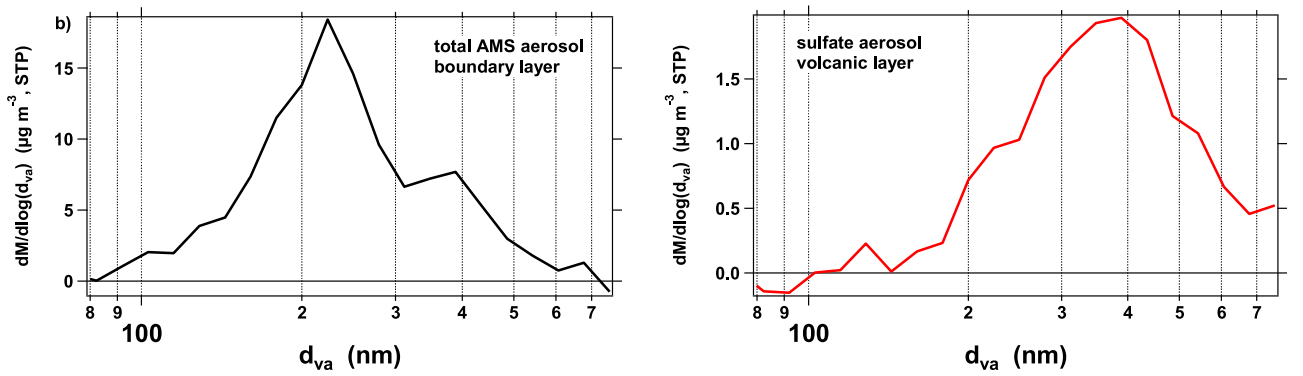

Figure 10. (continued)

aerosol layer within the UT/LS region are shown separately from the background values (first panel versus second panel in Figure 10a). In the boundary layer, the average mass concentration of submicron aerosol is 3.6 μg m^{-3} (STP) with the strongest contributions from nitrate, organics, and ammonium. This aerosol type is rather alkaline with an acidity coefficient larger than one (defined as the molar equivalence ratio (ER) of measured ammonium and the sum of measured sulfate and nitrate, all in μmol m^{-3}, see *Quinn et al.* [2006]). Alkaline boundary layer aerosol has been observed on other occasions, as well [*Martin et al.*, 2008]. In the free troposphere the composition changes, almost 50% mass contribution from particulate sulfate makes the aerosol more acidic than in the boundary layer, and no nitrate is found. Furthermore, the average concentration decreases by a factor of 12 to 0.3 μg m^{-3}. The UT/LS region is very similar in aerosol mass and composition to the free troposphere. However, during volcanic aerosol encounters both characteristics change. Relative mass contributions are 71%, 8% and 21%, sulfate, ammonium and organics, respectively. This results in an acidity coefficient of 0.29. The average mass concentration within the encountered layer was 1.2 μg m^{-3} (STP), a third of the boundary layer mass concentration.

[38] Additional information is obtained from the organic mass spectra that are displayed in Figure 10a. The error bars denote uncertainties from counting statistics and gray bars represent values below detection limit. Near the surface, the mass spectrum shows the typical sequence of uneven m/z, as pointed out in Figure 10a (fourth panel), representing hydrocarbon-like organic aerosol (HOA) [*Zhang et al.*, 2005] that is observed in fossil fuel combustion [*Schneider et al.*, 2006b]. This signature might come from the emissions of the Falcon's engines in addition to regular road traffic emissions from nearby sources. Furthermore, oxygenated organic aerosol (OOA) is present indicated by a high m/z 44 (CO_2^+) peak [*Zhang et al.*, 2005]. The m/z 44 over total organics (OA) ratio as indicator of oxygenation is 0.11 ± 0.002. The error denotes the 95% confidence interval of the linear regression fit of m/z 44 versus OA. Applying the linear regression equation for elemental O/C ratio versus m/z 44 over OA as suggested by *Aiken et al.* [2008], the equivalent elemental ratio would be 0.50 ± 0.025. Such organic aerosol mass spectra have been identified as urban oxygenated organic aerosol [*Alfarra et al.*, 2004; *Zhang et al.*, 2005]. At higher altitudes the organic aerosol is found to be oxygenated to a much higher degree. The m/z 44/OA ratio increases from 0.16 ± 0.003 (0.69 ± 0.022, equivalent O/C) in the free troposphere to 0.21 ± 0.004 (0.88 ± 0.019, equivalent O/C) in the upper troposphere and lower stratosphere, where m/z 29 makes up 45%, and m/z 44 contributes 21% to the total organic mass. Although the contribution of m/z 29 is higher than observed in other data, such organic mass spectra can be identified with the type "OOA-1" [*Lanz et al.*, 2007; *Ulbrich et al.*, 2009] or "LV-OOA" (low-volatile OOA) [*Jimenez et al.*, 2009] and similar mass spectra have been observed in the free troposphere before [*Hock et al.*, 2008]. In the volcanic aerosol layer, the ratio is slightly lower with 0.16 ± 0.003 (0.69 ± 0.021, equivalent O/C).

[39] In Figure 11 a schematic vertical profile of organic and sulfate aerosol concentrations is shown distinguishing between loadings in the free troposphere, background UT/LS and volcanic layer. The absolute concentration of organic material in the volcanic layer was found to be a factor 1.4 times higher than in the background UT/LS, namely 0.25 ± 0.12 versus 0.18 ± 0.11 μg m^{-3}, respectively. Compared to the free troposphere, an enhancement factor of 1.9 in mass was observed. Even though the increase in organic aerosol mass is not significant within the one standard deviation boundaries, the trend is clearly visible from Figure 11. It is

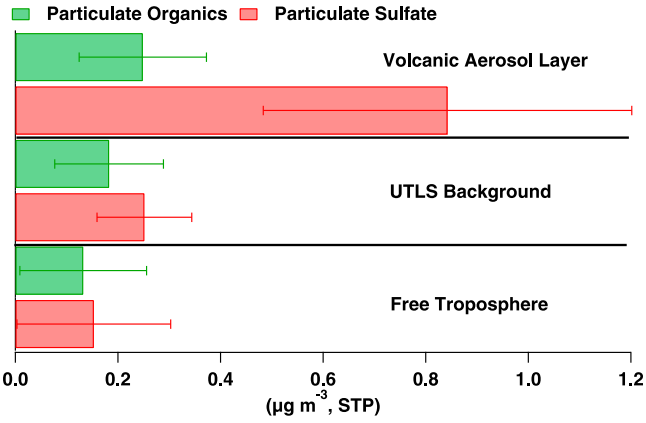

Figure 11. Average concentration of particulate organics and sulfate including one standard deviation.

possible that the AMS collection efficiency increased during plume encounters due to the dominant presence of sulfuric acid [*Quinn et al.*, 2006] and that therefore the increase in mass of organic compounds might not be real. However, the general composition of UT/LS aerosol within and outside of volcanic plumes does not change much with respect to its composition of mainly particulate sulfate and organics. Thus, a significant change in the *CE* is not expected. Overall, the quantification of organic material in the volcanic plume is subject to uncertainties so that we cannot state whether there is a true increase in organics. Nevertheless, these findings suggest that the volcanic aerosol contained also carbonaceous material, a finding that has also been reported by *Martinsson et al.* [2009].

[40] It is unclear whether the apparent increase in carbonaceous mass might reflect injection of volcanic species or injection of tropospheric species which experienced entrainment into the eruption column and thereafter participated in rapid injection into the LS. It is unlikely that the excess organic aerosol is due to entrainment of ambient stratospheric organic aerosol particles in the volcanic plume, because the organic aerosol mass concentration in the plume is slightly higher than in the background. However, it is conceivable that semivolatile and low-volatile organic compounds of tropospheric origin have contributed to the formation and growth of the particles in the lower stratosphere. Similarly *Ekman et al.* [2008] found for tropical upper tropospheric aerosol in new particle formation events that organics seem to play a role besides sulfate in the formation and growth of small particles. This also has implications on the efficiency of heterogeneous reaction rates which can occur in/on volcanic aerosols because usually for the corresponding calculations reactive uptake coefficients are adopted assuming the volcanic particles to consist of pure binary sulfuric acid solution droplets [*Borrmann et al.*, 1997; *Fahey et al.*, 1993; *Keim et al.*, 1996]. The observed presence of a significant organic component of about 20% may substantially influence the reactive uptake.

3.3. Size Distributions

[41] Figure 10b shows mass size distributions recorded in the boundary layer and in the volcanic aerosol layer. The boundary layer data were obtained shortly before landing on 28 October and 2 November and shortly after takeoff on 29 October. Figure 10b (left) shows the average distribution for the sum of all chemical components. The size distribution is bimodal: The smaller mode has a mode diameter of about 220 nm d_{va} and the second mode has a mode diameter of about 400 nm. The resolution is 25 bins between 50 and 800 nm d_{va}. The vacuum aerodynamic diameter can be converted into mobility diameter (d_{mob}) after *DeCarlo et al.* [2004] by dividing d_{va} by the density of the aerosol and its shape factor. Assuming spherical shape and a density of 1.7 g cm^{-3} for the inorganic fraction and 1 g cm^{-3} for the organic fraction, the mode diameters correspond to 150 and 260 nm d_{mob}. For the free troposphere and UT/LS region no size distribution could be obtained due to the low mass concentrations. In the volcanic aerosol layer, the mass size distribution is dominated by particulate sulfate (see Figure 10b, right). The mass size distribution has a mode diameter at approximately 360 nm d_{va} and a geometric standard deviation of 1.4. According to *Wilson et al.* [1993] the volumetric size distribution of stratospheric aerosol 78 days after the Pinatubo eruption showed a mode diameter between 300 and 400 nm d_{mob} measured by a focused cavity aerosol spectrometer [*Jonsson et al.*, 1995]) for submicron aerosol. Converting our findings into d_{mob} by dividing 360 nm d_{va} by the density of sulfuric acid (1.84 g cm^3) and assuming spherical particle shape a mode diameter of approximately 200 nm d_{mob} is obtained. The fact that the Kasatochi aerosol seems to be smaller after a very similar period after the eruption (85 days compared to 78 days) may reflect the larger amount of sulfur dioxide injected into the stratosphere by Mount Pinatubo compared to Mount Kasatochi (20 Mt compared to 1.4 Mt), leading to higher particle formation and growth rates after the Pinatubo eruption. As mentioned above, the conversion of SO_2 to sulfate aerosol is almost complete (about 80%) after 85 days, see *Jurkat et al.* [2010].

4. Summary and Conclusion

[42] During the CONCERT campaign conducted between 27 October and 2 November 2008, high concentrations with a maximum of about 2.0 μg m^{-3} (STP) of submicron particulate sulfate were observed over the North Sea and North Atlantic Flight corridor. Relating these findings to various definitions (PV, O_3, CO-O_3) for the location of the tropopause we found that this aerosol layer was situated in the lower stratosphere, directly above the tropopause. Possible sources of the observed aerosol layer such as air traffic, OCS conversion, and vertical convective transport were ruled out. Thus, the most likely explanation is that the observed aerosol layer originated from the eruptions of Mount Okmok and Mount Kasatochi that erupted on 12 July and 7 August 2008, respectively, and transferred together more than 1.6 Tg SO_2 into the stratosphere. Data records from two German lidar stations at Kühlungsborn and Leipzig support the conclusion that volcanic aerosol has been observed since they detected lower stratospheric aerosol layers from shortly after the eruption to after the CONCERT campaign. According to meteorological data, potential vorticity and trace gases, the particulate sulfate layer was observed during CONCERT within a tropopause fold which explains its descent to approximately 8 km without entering the troposphere as measured on 31 October. Parallel measurement of sulfur dioxide aboard the Falcon showed that approximately 80% of gaseous sulfur had been converted into sulfate aerosol 85 days after the Mount Kasatochi eruption [*Jurkat et al.*, 2010]. The volcanic aerosol was found to be composed of 71% sulfate, 21% highly oxygenated organic matter and 8% ammonium. These measurements represent to our knowledge the first detection of stratospheric volcanic aerosol by an aerosol mass spectrometer. The origin of the carbonaceous components in the volcanic aerosol that were also reported by *Martinsson et al.* [2009] remains an open question. It is conceivable that the volcanic eruption column injected air from the troposphere that contained also organic precursor gases that contributed to the formation and growth of the observed particles. Due to the lack of comparable data from previous volcanic eruptions, this question remains unanswered, but the finding that volcanic aerosol contains also

Table A1. PCI Specifications for the CONCERT and POLARCAT Campaign[a]

	CONCERT			POLARCAT
	PCI 1	PCI 2	PCI 3	PCI POLARCAT
Orifice 1 and 2 (μm)	380, 200	400, 200	380, 250	400, 160
Operated on	27 Oct 2008	28 Oct 2008 29 Oct 2008	31 Oct 2008 1 Nov 2008	30 June to 14 July 2008
High P_{amb} (hPa)	>800	>600	>600	
P_{PCI} function	$P_{PCI} = 0.22*P_{amb} + 2.76$	$P_{PCI} = 0.36*P_{amb} - 35.7$	$P_{PCI} = 0.29*P_{amb} - 73.2$	
P_{Lens} (hPa)	2.4–2.2	2.9–2.3	2.9–2.3	
Upper cutoff d_{va} (nm)	735	735	735	
Core P_{amb} (hPa)	800–295	600–200	600–180	1000–350
P_{PCI} function	$P_{PCI} = 190$	$P_{PCI} = 188$	$P_{PCI} = 110$	$P_{PCI} = 387$
P_{Lens} (hPa)	2.2	2.2	2.2	2.2
Upper cutoff d_{va} (nm)	800	800	800	800
Low P_{amb} (hPa)	<295	<200	<180	<350
P_{PCI} function	$P_{PCI} = 0.33*P_{amb} + 96.5$	$P_{PCI} = 0.58*P_{amb} + 69.5$	$P_{PCI} = 0.27*P_{amb} + 61.8$	$P_{PCI} = 0.89*P_{amb} + 53.5$
P_{Lens} (hPa)	<2.2	<2.2	<2.2	<2.2
Upper cutoff d_{va} (nm)	420	420	800	800

[a] P_{amb} is ambient pressure; P_{PCI} is pressure in the intermediate region; P_{Lens} is pressure in AMS lens. Core P_{amb} denotes ambient pressures when P_{PCI} is constant; high P_{amb} and low P_{amb} refer to ambient pressures that are too high or too low to keep P_{PCI} constant; P_{PCI} thus becomes a function of P_{amb}.

organic material might have important implications for heterogeneous reactions on volcanic stratospheric aerosol.

Appendix A: Pressure Controlled Inlet System Characterization

[43] The employed PCIs were built according to the design described by *Bahreini et al.* [2008]. The purpose of a PCI is to facilitate stable conditions in front of the AMS inlet lens to assure the operation of the aerodynamic lens under constant pressure. Pressure changes in front of the instrument's inlet lead to changes in the lens transmission function and to different acceleration velocities in the aerodynamic lens and thus to variability in particle sizing and transmission efficiency. Therefore, an intermediate region, consisting of a 210 mm long 9.5 mm ID stainless steel tube, located between the critical orifice at the aerodynamic lens entrance and another one upstream of it is kept at a constant pressure so that the mass flow remains constant, as well. This is realized by a PID controlled valve which is coupled via a feedback loop to a pressure sensor reporting the AMS lens pressure (P_{Lens}). If P_{Lens} exceeds the target value at lower altitudes the valve allows more air to be withdrawn from the intermediate region. If P_{Lens} drops below the target value at higher altitudes, the valve reduces the throughput and the intermediate pressure (P_{PCI}) stabilizes again. Before the excess air is withdrawn symmetrically from both sides of the half inch tube, a 1.9 mm ID tube of 750 mm length connected directly to the AMS lens inlet samples the aerosol at a distance of 105 mm from the upstream orifice. For a schematic drawing of a PCI see *Bahreini et al.* [2008]. During the POLARCAT campaign this PCI design was modified by introducing a sampling line to a CPC (TSI 3010) in the intermediate chamber after the withdrawal of AMS sampling air, so that the flow into the PCI was 1.74 l/min.

[44] P_{PCI} was aimed to be kept at half the lowest expected ambient pressure for a maximum flight altitude of 12 km. To meet the requirements of a PCI operating between pressures of approximately 950 and 200 hPa the combination of critical orifices was adapted various times during the CONCERT campaign. Table A1 shows the respective intermediate pressures, lens pressures and size cutoffs for both campaigns. The cutoffs were derived by introducing PSL (polystyrene latex spheres) of defined size through the PCI into the AMS. The signal for m/z 104 (mass to charge ratio), dominant for PSL, was plotted against time of flight in the vacuum chamber. When no signal could be observed the cutoff was assumed to be between the current and biggest particle size giving a signal. Generally, the PCI allowed detection for particles between 84 and 735 nm d_{va}; however, very low ambient pressure forced the cutoff partially down to approximately 400 nm d_{va}. This is most likely caused by a combination of two effects: First, lower lens pressure leads to less acceleration within the particle time-of-flight region in the vacuum chamber, and thus, the flight time exceeds the threshold of the electronic acquisition settings. Second, lower lens pressures allow bigger particles not to follow the gas streamlines so that they strike the inner surfaces of the lens. The pressure regime where P_{PCI} was kept constant by the regulation is termed "core P_{amb}." For ambient pressures outside of the core P_{amb} regime, P_{PCI} is a function of P_{amb}. These pressure regions are termed "high P_{amb}" and "low P_{amb}." Size calibrations for each PCI were performed at different P_{Lens}. Thus, size distributions could be determined for all flight altitudes and lens pressures.

[45] For correct quantification of particle mass, the transmission efficiency of the PCI was determined in laboratory experiments. For particles larger than 400 nm d_{va} (PSL) the transmission efficiency was determined by particle counting using the integrated light scattering probe (LSP) [*Cross et al.*, 2007], for particles smaller than 400 nm d_{va} (NH_4NO_3, ammonium nitrate particles) the transmission was measured by the mass method as described by *Liu et al.* [2007]. The experiments were conducted for the standard AMS inlet and the four versions of the PCI coupled to the standard inlet. Both methods include both PCI and aerodynamic lens transmission. The results are shown in Figure 1.

[46] For the three PCIs with the second critical orifice greater than 160 μm (PCI 1 to 3) the transmission efficiency is the same as for the standard inlet within the calculated error range. For LSP measurements, the error represents the standard deviation of 1 min averaged CPC counts over LSP counts for the total number of collected data points (between 15 and 20). For mass method measurements, the

error accounts for variations in the charge probability of the monodisperse aerosol and the counting statistics for determination of AMS nitrate mass. Generally, transmission between 200 and 400 nm d_{va} particles for the PCI used in POLARCAT and between 200 and 600 nm for all other inlets is close to 100%. Thus, the respective data of the CONCERT campaign have not been corrected for differences in inlet transmission. The POLARCAT inlet shows lower transmission for particle sizes smaller than 200 nm d_{va} and larger than 400 nm resulting in an overall inlet transmission of approximately 54% compared to the standard inlet. Mass concentrations from POLARCAT have been corrected accordingly. Generally, PCIs with a larger second orifice have higher transmission for small and large particles and are similar to the standard inlet.

[47] **Acknowledgments.** We acknowledge funding by the German Research Foundation (DFG) through the SPP 1294, by the "Exzellenzcluster Geocycles," and by the Max Planck Society. We also thank the AEROTROP junior research group for organizing the CONCERT campaign and the Falcon crew for assistance during measurements. The Falcon flights were funded by the DLR project CATS. POLARCAT-France gratefully acknowledges funding from the following French research agencies: ANR, CNES, CNRS-INSU, IPEV, and EUFAR, and we thank the ATR-42 crew for their support. Heike Eichler was funded under the Collaborative Research Center 641: TROPICE "The Tropospheric Ice Phase." We also would like to thank the ARCTAS team, especially Michael Cubison and Jose Jimenez (CU Boulder) for providing their data. The EARLINET-ASOS project is funded by the European Commission (EC) under grant RICA-025991. The authors gratefully acknowledge the NOAA Air Resources Laboratory (ARL) for the provision of the HYSPLIT transport and dispersion model and READY Web site (http://www.arl.noaa.gov/ready.html) used in this publication. We also thank Michael Cubison for sharing AMS fast mode analysis routines. Many thanks go also to Friederike Freutel for helping with the LSP data analysis and to Marco Brands for his great support during the POLARCAT campaign.

References

Aiken, A. C., et al. (2008), O/C and OM/OC ratios of primary, secondary, and ambient organic aerosols with high-resolution time-of-flight aerosol mass spectrometry, *Environ. Sci. Technol.*, *42*(12), 4478–4485, doi:10.1021/es703009q.

Alfarra, M. R., et al. (2004), Characterization of urban and rural organic particulate in the lower Fraser valley using two Aerodyne aerosol mass spectrometers, *Atmos. Environ.*, *38*(34), 5745–5758, doi:10.1016/j.atmosenv.2004.01.054.

Allan, J. D., J. L. Jimenez, P. I. Williams, M. R. Alfarra, K. N. Bower, J. T. Jayne, H. Coe, and D. R. Worsnop (2003), Quantitative sampling using an Aerodyne aerosol mass spectrometer: 1. Techniques of data interpretation and error analysis, *J. Geophys. Res.*, *108*(D3), 4090, doi:10.1029/2002JD002358.

Allan, J. D., et al. (2004a), Submicron aerosol composition at Trinidad Head, California, during ITCT 2K2: Its relationship with gas phase volatile organic carbon and assessment of instrument performance, *J. Geophys. Res.*, *109*, D23S24, doi:10.1029/2003JD004208.

Allan, J. D., et al. (2004b), A generalised method for the extraction of chemically resolved mass spectra from Aerodyne aerosol mass spectrometer data, *J. Aerosol Sci.*, *35*(7), 909–922, doi:10.1016/j.jaerosci.2004.02.007.

Ancellet, G., J. Leclair de Bellevue, C. Mari, P. Nedelec, A. Kukui, A. Borbon, and P. Perros (2009), Effects of regional-scale and convective transports on tropospheric ozone chemistry revealed by aircraft observation during the wet season of the AMMA campaign, *Atmos. Chem. Phys.*, *9*, 383–411, doi:10.5194/acp-9-383-2009.

Arnold, F., T. Buhrke, and S. Qiu (1990), Evidence for stratospheric ozone-depleting heterogeneous chemistry on volcanic aerosols from El-Chichon, *Nature*, *348*(6296), 49–50, doi:10.1038/348049a0.

Arnold, F., J. Curtius, S. Spreng, and T. Deshler (1998), Stratospheric aerosol sulfuric acid: First direct in situ measurements using a novel balloon-based mass spectrometer apparatus, *J. Atmos. Chem.*, *30*(1), 3–10, doi:10.1023/A:1006067511568.

Bahreini, R., J. L. Jimenez, J. Wang, R. C. Flagan, J. H. Seinfeld, J. T. Jayne, and D. R. Worsnop (2003), Aircraft-based aerosol size and composition measurements during ACE-Asia using an Aerodyne aerosol mass spectrometer, *J. Geophys. Res.*, *108*(D23), 8645, doi:10.1029/2002JD003226.

Bahreini, R., E. J. Dunlea, B. M. Matthew, C. Simons, K. S. Docherty, P. F. DeCarlo, J. L. Jimenez, C. A. Brock, and A. M. Middlebrook (2008), Design and operation of a pressure-controlled inlet for airborne sampling with an aerodynamic aerosol lens, *Aerosol Sci. Technol.*, *42*, 465–471, doi:10.1080/02786820802178514.

Borrmann, S., J. E. Dye, D. Baumgardner, J. C. Wilson, H. H. Jonsson, C. A. Brock, M. Loewenstein, J. R. Podolske, G. V. Ferry, and K. S. Barr (1993), In-situ measurements of changes in stratospheric aerosol and the N_2O-aerosol relationship inside and outside of the polar vortex, *Geophys. Res. Lett.*, *20*(22), 2559–2562, doi:10.1029/93GL01694.

Borrmann, S., et al. (1995), Aerosols as dynamical tracers in the lower stratosphere: Ozone versus aerosol correlation after the Mount Pinatubo eruption, *J. Geophys. Res.*, *100*(D6), 11,147–11,156, doi:10.1029/95JD00016.

Borrmann, S., S. Solomon, J. E. Dye, and B. P. Luo (1996), The potential of cirrus clouds for heterogeneous chlorine activation, *Geophys. Res. Lett.*, *23*(16), 2133–2136, doi:10.1029/96GL01957.

Borrmann, S., S. Solomon, J. E. Dye, D. Baumgardner, K. K. Kelly, and K. R. Chan (1997), Heterogeneous reactions on stratospheric background aerosols, volcanic sulfuric acid droplets, and type I polar stratospheric clouds: Effects of temperature fluctuations and differences in particle phase, *J. Geophys. Res.*, *102*(D3), 3639–3648, doi:10.1029/96JD02976.

Borrmann, S., et al. (2010), Aerosols in the tropical und subtropical UT/LS: In-situ measurements of ultrafine particle abundance and volatility, *Atmos. Chem. Phys.*, *10*, 5573–5592, doi:10.5194/acp-10-5573-2010.

Brenguier, J.-L., L. Gomes, T. Bourrianne, R. Caillou, A. Gribkoff, P. Nacass, P. Laj, P. Villani, and D. Piccard (2008), Community aerosol inlet, paper presented at Workshop on Aircraft Instrumentation, Aerial Vehicles Program, Atmos. Radiat. Measure. Program, Urbana-Champaign, Ill.

Brough, N., et al. (2003), Intercomparison of aircraft instruments on board the C-130 and Falcon 20 over southern Germany during EXPORT 2000, *Atmos. Chem. Phys.*, *3*, 2127–2138, doi:10.5194/acp-3-2127-2003.

Canagaratna, M. R., et al. (2007), Chemical and microphysical characterization of ambient aerosols with the Aerodyne aerosol mass spectrometer, *Mass Spectrom. Rev.*, *26*(2), 185–222, doi:10.1002/mas.20115.

Carn, S. A., N. A. Krotkov, V. Fioletov, K. Yang, A. J. Krueger, and D. Tarasick (2008), Emission, transport and validation of sulfur dioxide in the 2008 Okmok and Kasatochi eruption clouds, *Eos Trans. AGU*, *89*(53), Fall Meet. Suppl., Abstract A51J-07.

Crosier, J., J. D. Allan, H. Coe, K. N. Bower, P. Formenti, and P. I. Williams (2007), Chemical composition of summertime aerosol in the Po Valley (Italy), northern Adriatic and Black Sea, *Q. J. R. Meteorol. Soc.*, *133*, 61–75, doi:10.1002/qj.88.

Cross, E. S., J. G. Slowik, P. Davidovits, J. D. Allan, D. R. Worsnop, J. T. Jayne, D. K. Lewis, M. Canagaratna, and T. B. Onasch (2007), Laboratory and ambient particle density determinations using light scattering in conjunction with aerosol mass spectrometry, *Aerosol Sci. Technol.*, *41*, 343–359, doi:10.1080/02786820701199736.

DeCarlo, P. F., J. G. Slowik, D. R. Worsnop, P. Davidovits, and J. L. Jimenez (2004), Particle morphology and density characterization by combined mobility and aerodynamic diameter measurements. Part 1: Theory, *Aerosol Sci. Technol.*, *38*, 1185–1205, doi:10.1080/027868290903907.

DeCarlo, P. F., et al. (2008), Fast airborne aerosol size and chemistry measurements above Mexico City and Central Mexico during the MILAGRO campaign, *Atmos. Chem. Phys.*, *8*, 4027–4048, doi:10.5194/acp-8-4027-2008.

Deshler, T. (2008), A review of global stratospheric aerosol: Measurements, importance, life cycle, and local stratospheric aerosol, *Atmos. Res.*, *90*(2–4), 223–232, doi:10.1016/j.atmosres.2008.03.016.

Draxler, R. R., and G. D. Rolph (2003), HYSPLIT—Hybrid Single-Particle Lagrangian Integrated Trajectory Model, NOAA Air Resour. Lab., Silver Spring, Md. (Available at, http://www.arl.noaa.gov/ready/hysplit4.html)

Drewnick, F., J. J. Schwab, J. T. Jayne, M. Canagaratna, D. R. Worsnop, and K. L. Demerjian (2004), Measurement of ambient aerosol composition during the PMTACS-NY 2001 using an aerosol mass spectrometer. Part I: Mass concentrations, *Aerosol Sci. Technol.*, *38*, 92–103, doi:10.1080/02786820390229507.

Drewnick, F., et al. (2005), A new time-of-flight aerosol mass spectrometer (TOF-AMS)—Instrument description and first field deployment, *Aerosol Sci. Technol.*, *39*, 637–658, doi:10.1080/02786820500182040.

Drewnick, F., S. S. Hings, M. R. Alfarra, A. S. H. Prevot, and S. Borrmann (2009), Aerosol quantification with the Aerodyne aerosol mass spectrometer: Detection limits and ionizer background effects, *Atmos. Meas. Tech.*, *2*, 33–46, doi:10.5194/amt-2-33-2009.

Dunlea, E. J., et al. (2009), Evolution of Asian aerosols during transpacific transport in INTEX-B, *Atmos. Chem. Phys.*, *9*, 7257–7287, doi:10.5194/acp-9-7257-2009.

Ehrlich, A., E. Bierwirth, M. Wendisch, J. F. Gayet, G. Mioche, A. Lampert, and J. Heintzenberg (2008), Cloud phase identification of Arctic boundary-layer clouds from airborne spectral reflection measurements: Test of three approaches, *Atmos. Chem. Phys.*, *8*, 7493–7505, doi:10.5194/acp-8-7493-2008.

Eichler, H., A. Ehrlich, M. Wendisch, G. Mioche, J. F. Gayet, M. Wirth, C. Emde, and A. Minikin (2009), Influence of ice crystal shape on retrieval of cirrus optical thickness and effective radius: A case study, *J. Geophys. Res.*, *114*, D19203, doi:10.1029/2009JD012215.

Ekman, A. M. L., R. Krejci, A. Engstrom, J. Strom, M. de Reus, J. Williams, and M. O. Andreae (2008), Do organics contribute to small particle formation in the Amazonian upper troposphere?, *Geophys. Res. Lett.*, *35*, L17810, doi:10.1029/2008GL034970.

Fahey, D. W., et al. (1993), In situ measurements constraining the role of sulfate aerosols in mid-latitude ozone depletion, *Nature*, *363*(6429), 509–514, doi:10.1038/363509a0.

Fiebig, M. (2001), The tropospheric aerosol at mid-latitudes—Microphysics, optics, and climate forcing illustrated by the LACE 98 field study (in German), Ph.D. thesis, Univ. of Munich, Munich, Germany.

Fiedler, V., et al. (2005), The contribution of sulphuric acid to atmospheric particle formation and growth: A comparison between boundary layers in northern and central Europe, *Atmos. Chem. Phys.*, *5*, 1773–1785, doi:10.5194/acp-5-1773-2005.

Fiedler, V., R. Nau, S. Ludmann, F. Arnold, H. Schlager, and A. Stohl (2009), East Asian SO_2 pollution over Europe—Part 1: Airborne trace gas measurements and source identification by particle dispersion model simulations, *Atmos. Chem. Phys.*, *9*, 4717–4728, doi:10.5194/acp-9-4717-2009.

Fischer, H., F. G. Wienhold, P. Hoor, O. Bujok, C. Schiller, P. Siegmund, M. Ambaum, H. A. Scheeren, and J. Lelieveld (2000), Tracer correlations in the northern high latitude lowermost stratosphere: Influence of cross-tropopause mass exchange, *Geophys. Res. Lett.*, *27*(1), 97–100, doi:10.1029/1999GL010879.

Froyd, K. D., D. M. Murphy, P. Lawson, D. Baumgardner, and R. L. Herman (2009a), Composition of cirrus-forming aerosols at the tropical tropopause, *Atmos. Chem. Phys. Discuss.*, *9*, 20,347–20,369, doi:10.5194/acpd-9-20347-2009.

Froyd, K. D., D. M. Murphy, T. J. Sanford, D. S. Thomson, J. C. Wilson, L. Pfister, and L. Lait (2009b), Aerosol composition of the tropical upper troposphere, *Atmos. Chem. Phys.*, *9*, 4363–4385, doi:10.5194/acp-9-4363-2009.

Griffiths, P. T., C. L. Badger, R. A. Cox, M. Folkers, H. H. Henk, and T. F. Mentel (2009), Reactive uptake of N_2O_5 by aerosols containing dicarboxylic acids. Effect of particle phase, composition, and nitrate content, *J. Phys. Chem. A*, *113*(17), 5082–5090, doi:10.1021/jp8096814.

Hinds, C. (1999), *Aerosol Technology: Properties, Behavior, and Measurement of Airborne Particles*, John Wiley, New York.

Hings, S. S., S. Walter, J. Schneider, S. Borrmann, and F. Drewnick (2007), Comparison of a quadrupole and a time-of-flight aerosol mass spectrometer during the Feldberg Aerosol Characterization Experiment 2004, *Aerosol Sci. Technol.*, *41*, 679–691, doi:10.1080/02786820701408483.

Hock, N., J. Schneider, S. Borrmann, A. Rompp, G. Moortgat, T. Franze, C. Schauer, U. Poschl, C. Plass-Dulmer, and H. Berresheim (2008), Rural continental aerosol properties and processes observed during the Hohenpeissenberg Aerosol Characterization Experiment (HAZE2002), *Atmos. Chem. Phys.*, *8*, 603–623, doi:10.5194/acp-8-603-2008.

Holton, J. R., P. H. Haynes, M. E. McIntyre, A. R. Douglass, R. B. Rood, and L. Pfister (1995), Stratosphere-troposphere exchange, *Rev. Geophys.*, *33*(4), 403–439, doi:10.1029/95RG02097.

Huffman, J. A., J. T. Jayne, F. Drewnick, A. C. Aiken, T. Onasch, D. R. Worsnop, and J. L. Jimenez (2005), Design, modeling, optimization, and experimental tests of a particle beam width probe for the Aerodyne aerosol mass spectrometer, *Aerosol Sci. Technol.*, *39*, 1143–1163, doi:10.1080/02786820500423782.

Hunton, D. E., et al. (2005), In-situ aircraft observations of the 2000 Mt. Hekla volcanic cloud: Composition and chemical evolution in the arctic lower stratosphere, *J. Volcanol. Geotherm. Res.*, *145*(1–2), 23–34, doi:10.1016/j.jvolgeores.2005.01.005.

Jimenez, J. L., et al. (2009), Evolution of organic aerosols in the atmosphere, *Science*, *326*(5959), 1525–1529, doi:10.1126/science.1180353.

Jonsson, H. H., et al. (1995), Performance of a focused cavity aerosol spectrometer for measurements in the stratosphere of particle-size in the 0.06–2.0-μm-diameter range, *J. Atmos. Oceanic Technol.*, *12*(1), 115–129, doi:10.1175/1520-0426(1995)012<0115:POAFCA>2.0.CO;2.

Jurkat, T., C. Voigt, F. Arnold, H. Schlager, H. Aufmhoff, J. Schmale, J. Schneider, M. Lichtenstern, A. Dörnbrack (2010), Airborne stratospheric ITCIMS measurements of SO_2, HCl, and HNO_3 in the aged plume of volcano Kasatochi, *J. Geophys. Res.*, doi:10.1029/2010JD013890, in press.

Keim, E. R., et al. (1996), Observations of large reductions in the NO/NOy ratio near the mid-latitude tropopause and the role of heterogeneous chemistry, *Geophys. Res. Lett.*, *23*(22), 3223–3226, doi:10.1029/96GL02593.

Kimmel, J. R., D. K. Farmer, D. Sueper, M. Cubison, C. Tanner, and J.-L. Jimenez (2008), Monitoring of fast changes in aerosol chemistry with a time-of-flight aerosol mass spectrometer, poster presented at 56th Conference on Mass Spectrometry and Allied Topics, Am. Soc. For Mass. Spectrom., Denver, Colo.

Krueger, A., N. Krotkov, and S. Carn (2008), El Chichon: The genesis of volcanic sulfur dioxide monitoring from space, *J. Volcanol. Geotherm. Res.*, *175*(4), 408–414, doi:10.1016/j.jvolgeores.2008.02.026.

Lanz, V. A., M. R. Alfarra, U. Baltensperger, B. Buchmann, C. Hueglin, and A. S. H. Prevot (2007), Source apportionment of submicron organic aerosols at an urban site by factor analytical modelling of aerosol mass spectra, *Atmos. Chem. Phys.*, *7*, 1503–1522, doi:10.5194/acp-7-1503-2007.

Liu, P. S. K., R. Deng, K. A. Smith, L. R. Williams, J. T. Jayne, M. R. Canagaratna, K. Moore, T. B. Onasch, D. R. Worsnop, and T. Deshler (2007), Transmission efficiency of an aerodynamic focusing lens system: Comparison of model calculations and laboratory measurements for the Aerodyne aerosol mass spectrometer, *Aerosol Sci. Technol.*, *41*, 721–733, doi:10.1080/02786820701422278.

Marcy, T. P., R. S. Gao, M. J. Northway, H. Stark, and D. W. Fahey (2005), Using chemical ionization mass spectrometry for detection of HNO_3, HCl and $ClONO_2$ in the atmosphere, *Int. J. Mass Spectrom.*, *243*, 63–70, doi:10.1016/j.ijms.2004.11.012.

Martin, R. S., P. J. Silva, K. Moore, M. Erupe, and V. S. Doshi (2008), Particle composition and size distributions in and around a deep-pit swine operation, Ames, IA, *J. Atmos. Chem.*, *59*(2), 135–150, doi:10.1007/s10874-008-9097-y.

Martinsson, B. G., G. Papaspiropoulos, J. Heintzenberg, and M. Hermann (2001), Fine mode particulate sulphur in the tropopause region measured from intercontinental flights (CARIBIC), *Geophys. Res. Lett.*, *28*(7), 1175–1178, doi:10.1029/2000GL012257.

Martinsson, B. G., H. N. Nguyen, C. A. M. Brenninkmeijer, A. Zahn, J. Heintzenberg, M. Hermann, and P. F. J. van Velthoven (2005), Characteristics and origin of lowermost stratospheric aerosol at northern midlatitudes under volcanically quiescent conditions based on CARIBIC observations, *J. Geophys. Res.*, *110*, D12201, doi:10.1029/2004JD005644.

Martinsson, B. G., C. A. M. Brenninkmeijer, S. A. Carn, M. Hermann, K. P. Heue, P. F. J. van Velthoven, and A. Zahn (2009), Influence of the 2008 Kasatochi volcanic eruption on sulfurous and carbonaceous aerosol constituents in the lower stratosphere, *Geophys. Res. Lett.*, *36*, L12813, doi:10.1029/2009GL038735.

Matthew, B. M., A. M. Middlebrook, and T. B. Onasch (2008), Collection efficiencies in an Aerodyne aerosol mass spectrometer as a function of particle phase for laboratory generated aerosols, *Aerosol Sci. Technol.*, *42*, 884–898, doi:10.1080/02786820802356797.

Morgan, W. T., J. D. Allan, K. N. Bower, G. Capes, J. Croiser, P. I. Williams, and H. Coe (2009), Vertical distribution of sub-micron aerosol chemical composition from north-western Europe and the north-east Atlantic, *Atmos. Chem. Phys.*, *9*, 5389–5401, doi:10.5194/acp-9-5389-2009.

Murphy, D. M., D. S. Thomson, and T. M. J. Mahoney (1998), In situ measurements of organics, meteoritic material, mercury, and other elements in aerosols at 5 to 19 kilometers, *Science*, *282*(5394), 1664–1669, doi:10.1126/science.282.5394.1664.

Ovadnevaite, J., et al. (2009), Volcanic sulphate and arctic dust plumes over the North Atlantic Ocean, *Atmos. Environ.*, *43*(32), 4968–4974, doi:10.1016/j.atmosenv.2009.07.007.

Pan, L. L., W. J. Randel, B. L. Gary, M. J. Mahoney, and E. J. Hintsa (2004), Definitions and sharpness of the extratropical tropopause: A trace gas perspective, *J. Geophys. Res.*, *109*, D23103, doi:10.1029/2004JD004982.

Popp, P. J., et al. (2007), Condensed-phase nitric acid in a tropical subvisible cirrus cloud, *Geophys. Res. Lett.*, *34*, L24812, doi:10.1029/2007GL031832.

Quinn, P. K., et al. (2006), Impacts of sources and aging on submicrometer aerosol properties in the marine boundary layer across the Gulf of Maine, *J. Geophys. Res.*, *111*, D23S36, doi:10.1029/2006JD007582.

Rose, W. I., et al. (2006), Atmospheric chemistry of a 33–34 hour old volcanic cloud from Hekla volcano (Iceland): Insights from direct sampling and the application of chemical box modeling, *J. Geophys. Res.*, *111*, D20206, doi:10.1029/2005JD006872.

Sander, S. P., et al. (2006), Chemical kinetic and photochemical data for use in atmospheric studies, *Eval. 15, JPL Publ. 06-2*, Jet Propul. Lab., Pasadena, Calif.

Schneider, J., S. S. Hings, B. N. Hock, S. Weimer, S. Borrmann, M. Fiebig, A. Petzold, R. Busen, and B. Karcher (2006a), Aircraft-based operation of an aerosol mass spectrometer: Measurements of tropospheric aerosol composition, *J. Aerosol Sci.*, *37*(7), 839–857, doi:10.1016/j.jaerosci.2005.07.002.

Schneider, J., S. Weimer, F. Drewnick, S. Borrmann, G. Helas, P. Gwaze, O. Schmid, M. O. Andreae, and U. Kirchner (2006b), Mass spectrometric analysis and aerodynamic properties of various types of combustion-related aerosol particles, *Int. J. Mass Spectrom.*, *258*, 37–49, doi:10.1016/j.ijms.2006.07.008.

Schreiner, J., C. Voigt, P. Zink, D. Knopf, A. Kohlmann, and K. Mauersberger (2002), A mass spectrometer system for analysis of polar stratospheric aerosols, *Rev. Sci. Instrum.*, *73*, 446–452, doi:10.1063/1.1430732.

Smith, J. B., E. J. Hintsa, N. T. Allen, R. M. Stimpfle, and J. G. Anderson (2001), Mechanisms for midlatitude ozone loss: Heterogeneous chemistry in the lowermost stratosphere?, *J. Geophys. Res.*, *106*(D1), 1297–1309, doi:10.1029/2000JD900464.

Solomon, S., S. Borrmann, R. R. Garcia, R. Portmann, L. Thomason, L. R. Poole, D. Winker, and M. P. McCormick (1997), Heterogeneous chlorine chemistry in the tropopause region, *J. Geophys. Res.*, *102*(D17), 21,411–21,429, doi:10.1029/97JD01525.

Speidel, M., R. Nau, F. Arnold, H. Schlager, and A. Stohl (2007), Sulfur dioxide measurements in the lower, middle and upper troposphere: Deployment of an aircraft-based chemical ionization mass spectrometer with permanent in-flight calibration, *Atmos. Environ.*, *41*(11), 2427–2437, doi:10.1016/j.atmosenv.2006.07.047.

Theys, N., M. Van Roozendael, B. Dils, F. Hendrick, N. Hao, and M. De Maziere (2009), First satellite detection of volcanic bromine monoxide emission after the Kasatochi eruption, *Geophys. Res. Lett.*, *36*, L03809, doi:10.1029/2008GL036552.

Thomason, L., and T. Peter (Eds.) (2006), Assessment of stratospheric aerosol properties (ASAP), *WCRP-124, WMO/TD-1295, SPARC Rep. 4*, Stratospheric Processes and Their Role in Clim., Toronto, Ont., Canada.

Ulbrich, I. M., M. R. Canagaratna, Q. Zhang, D. R. Worsnop, and J. L. Jimenez (2009), Interpretation of organic components from positive matrix factorization of aerosol mass spectrometric data, *Atmos. Chem. Phys.*, *9*, 2891–2918, doi:10.5194/acp-9-2891-2009.

Voigt, C., et al. (2000), Nitric acid trihydrate (NAT) in polar stratospheric clouds, *Science*, *290*(5497), 1756–1758, doi:10.1126/science.290.5497.1756.

Voigt, C., H. Schlager, H. Ziereis, B. Karcher, B. P. Luo, C. Schiller, M. Kramer, P. J. Popp, H. Irie, and Y. Kondo (2006), Nitric acid in cirrus clouds, *Geophys. Res. Lett.*, *33*, L05803, doi:10.1029/2005GL025159.

Voigt, C., B. Karcher, H. Schlager, C. Schiller, M. Kramer, M. de Reus, H. Vossing, S. Borrmann, and V. Mitev (2007), In-situ observations and modeling of small nitric acid-containing ice crystals, *Atmos. Chem. Phys.*, *7*, 3373–3383, doi:10.5194/acp-7-3373-2007.

Voigt, C., et al. (2010), In-situ observations of young contrails—Overview and selected results from the CONCERT campaign, *Atmos. Chem. Phys. Discuss.*, *10*, 12,713–12,763, doi:10.5194/acpd-10-12713-2010.

von Glasow, R., N. Bobrowski, and C. Kern (2009), The effects of volcanic eruptions on atmospheric chemistry, *Chem. Geol.*, *263*, 131–142, doi:10.1016/j.chemgeo.2008.08.020.

Warneke, C., et al. (2006), Biomass burning and anthropogenic sources of CO over New England in the summer 2004, *J. Geophys. Res.*, *111*, D23S15, doi:10.1029/2005JD006878.

Wendisch, M., D. Muller, D. Schell, and J. Heintzenberg (2001), An airborne spectral albedometer with active horizontal stabilization, *J. Atmos. Oceanic Technol.*, *18*(11), 1856–1866, doi:10.1175/1520-0426(2001)018<1856:AASAWA>2.0.CO;2.

Wendisch, M., et al. (2008), Radiative and dynamic effects of absorbing aerosol particles over the Pearl River delta, China, *Atmos. Environ.*, *42*(25), 6405–6416, doi:10.1016/j.atmosenv.2008.02.033.

Wilson, J. C., et al. (1993), In situ observations of aerosol and chlorine monoxide after the 1991 eruption of Mount Pinatubo—Effect of reactions on sulfate aerosol, *Science*, *261*(5125), 1140–1143, doi:10.1126/science.261.5125.1140.

World Meteorological Organization (1999), Scientific assessment of ozone depletion: 1998, Global Ozone Res. and Monitoring Project, *Rep. 44*, WMO Global Ozone Obs. Syst., Geneva, Switzerland.

Zahn, A., and C. A. M. Brenninkmeijer (2003), New directions: A chemical tropopause defined, *Atmos. Environ.*, *37*(3), 439–440, doi:10.1016/S1352-2310(02)00901-9.

Zhang, Q., M. R. Alfarra, D. R. Worsnop, J. D. Allan, H. Coe, M. R. Canagaratna, and J. L. Jimenez (2005), Deconvolution and quantification of hydrocarbon-like and oxygenated organic aerosols based on aerosol mass spectrometry, *Environ. Sci. Technol.*, *39*(13), 4938–4952, doi:10.1021/es048568l.

G. Ancellet, LATMOS, Université Pierre et Marie Curie, CNRS, Tour 15, Aile 15-14-5e Etage, Boite 102, 4 place Jussieu, F-75252 Paris CEDEX 05, France.

F. Arnold, Max Planck Institute for Nuclear Physics, Saupfercheckweg 1, Postfach 103980, D-69117 Heidelberg, Germany.

S. Borrmann, J. Schmale, and J. Schneider, Particle Chemistry Department, Max Planck Institute for Chemistry, J.-J.-Becherweg 27, D-55128 Mainz, Germany. (julia.schmale@mpic.de)

M. Gerding, Leibniz Institute for Atmospheric Physics, Schloss-Str. 6, D-18225 Kühlungsborn, Germany.

T. Jurkat, M. Lichtenstern, M. Rautenhaus, H. Schlager, and C. Voigt, Deutsches Zentrum für Luft- und Raumfahrt, Institut für Physik der Atmosphäre, Münchner Straße 20, D-82234 Oberpfaffenhofen, Germany.

H. Kalesse, Institute for Atmospheric Physics, J. Gutenberg University, Becherweg 21, D-55099 Mainz, Germany.

I. Mattis, Leibniz Institute for Tropospheric Research, Permoserstr. 15, D-04318 Leipzig, Germany.

M. Wendisch, Institute of Meteorology, University of Leipzig, Permoserstr. 15, D-04318 Leipzig, Germany.